Summer 8-22-2021

Electrochemical Studies of Organic and Organometallic Compounds in the Pursuit of Electrocatalytic Carbon Dioxide Reduction

Joshua J. Ludtke
DePaul University, JLUDTKE@depaul.edu

Electrochemical Studies of Organic and Organometallic Compounds in the Pursuit of Electrocatalytic Carbon Dioxide Reduction

A Thesis

Submitted to the Faculty

of

DePaul University

by

Joshua J. Ludtke

In Partial Fulfillment of the

Requirements of the Degree

Of

Master of Science

March 2021

DePaul University

Chicago, Illinois

Acknowledgements

This work is dedicated to everyone who has kept me from giving up over the past half-dozen years: parents, extended family, friends, and professors; I would especially like to thank my partner Stephanie for being with me through the times I've had to work and struggle hardest, not only to work but to believe in myself.

Table of Contents

Table of Figures, Tables, and Schemes

Abstract

Carbon dioxide is the main contributor to the greenhouse effect in the world today; developing renewable energy sources and addressing anthropogenic CO_2 release into the atmosphere are two key ways of addressing its increasing impact. Electrocatalytic reduction to products like methanol or carbon monoxide is one useful path to address the rapid increase of carbon dioxide, and the *fac*-M(bpy-R)$(CO)_3$X family of complexes (M = Mn or Re; bpy-R = substituted 2,2'-bipyridine; X = Cl, Br, etc.) is one class of effective CO_2 reduction catalysts. Although the capability of the rhenium complex Re(PyBimH)$(CO)_3$Cl (PyBimH = 2-(2-pyridyl)benzimidazole) as a CO_2 reduction catalyst was previously determined to be minimal, the underlying reasons why were not explained, which is odd when considering that protic sites on the ligand have been shown to increase CO_2 reactivity. In this work, we show that the lack of electrocatalytic activity is due to a hydrogen atom transfer reaction that takes place upon reduction. In the process of testing for catalytic activity, a rapid method of determining the effective pK_a of acidic species in acetonitrile using cyclic voltammetry was discovered and explored. The pK_a of the rhenium complex was estimated through the cyclic voltammetry method to be 20 ± 1, in reasonable agreement with DFT calculations. Because determining acidity in non-aqueous solvents is not trivial using established methods, the discovery of a method to accurately estimate the pK_a of a species containing an acidic X-H bond is valuable. In addition to the organometallic rhenium complex, organic species buckminsterfullerene (C_{60}) and benzil were explored as viable catalysts for the electrochemical reduction of carbon dioxide. Buckminsterfullerene showed minor electrochemical activity in the presence of carbon dioxide as observed by cyclic voltammetry and infrared spectroelectrochemistry. In this study, cyclic voltammetry and infrared

spectroelectrochemistry showed that benzil reduces carbon dioxide at a lower overpotential than C_{60} and most other electrocatalysts. The production of oxalate from carbon dioxide by action of monoreduced benzil radical has been proposed, in agreement with literature. In the presence of pyridine, reactivity initially showed increased activity but did not show a linear trend in a quantified study of pyridine concentration.

Chapter 1. Electrochemical Investigations of *fac*-Re(PyBimH)(CO)$_3$Cl: Determining pK_a in Non-Aqueous Solvent

1.1. Introduction

Transformations involving protons and electrons are key to a renewable energy future.[1,2] Reducing protons to hydrogen, reducing carbon dioxide to carbon monoxide, and oxidizing water to oxygen gas all involve proton and electron transfers and are key steps in various approaches to artificial photosynthesis (Scheme 1.1). As a high impact field, progress in renewable energy—and improvements in storing energy chemically in particular—is a fruitful pursuit. Work in the Grice group has focused on electrochemical CO_2 reduction using homogenous electrocatalysts, and as such, understanding proton and electron transfer is of critical importance.[3-8]

Proton Reduction

$$2\,H^+ + 2\,e^- \longrightarrow H_2$$

Carbon Dioxide Reduction

$$CO_2 + 2\,H^+ + 2\,e^- \longrightarrow H_2O + CO$$

Water Oxidation

$$2\,H_2O \longrightarrow O_2 + 4\,H^+ + 4\,e^-$$

Scheme 1.1. Energy-important reactions that involve proton and electron transfers.

The movement of protons and electrons is broadly classified as proton-coupled electron transfer (PCET). In PCET, protons and electrons can transfer separately and in any PCET process, pK_a values and redox potentials are key values of merit as themodynamic quantities in proton and electron transfer processes. Another way of transferring protons and electrons is hydrogen atom

transfer (HAT), involving the transfer of a radical hydrogen between species, as shown in Scheme 1.2. In HAT, bond dissociation free energies (BDFE's) can be used to understand the overall energetics of the hydrogen atom transfer.

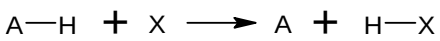

Scheme 1.3. A general Hydrogen Atom Transfer reaction scheme.

Classically, a single organic molecule that is a HAT acceptor will contain an unpaired electron, such as the radical species (2,2,6,6-tetramethylpiperidin-1-yl)oxyl (TEMPO) shown in Figure 1.1.[9]

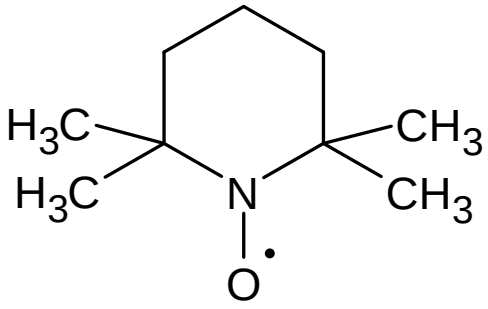

Figure 1.1. The structure of the stable (2,2,6,6-tetramethylpiperidin-1-yl)oxyl (TEMPO) radical and hydrogen atom acceptor.

In the case of organometallic complexes, different sites may play the parts of proton or electron acceptor in PCET, such as a proton going to a ligand and an electron going to the metal center.[9] BDFE's are a key thermodynamic parameter involved in analyzing HAT activity, but direct measurement of bond strength can be challenging.[10] However, HAT bond strengths can be

determined from redox and pK_a values of related species, as shown by the equation given in Warren and Mayer's review,[10] shown below in equation 1.

$$\mathrm{BDFE_{sol}(X-H)} = 1.37\mathrm{p}K_a + 23.06E^\circ + C_{\mathrm{G,sol}} \quad (1)$$

In equation 1, the pKa is the value of the H-X acidity in a given solvent, E° is the reduction potential of the radical X·, and $C_{\mathrm{g,sol}}$ is the $\mathrm{H^+/H^\circ}$ standard reduction potential within a given solvent, given as 54.9 kcal/mol in acetonitrile.[10] The relationship between pK_a, redox potentials, and BDFE can be seen in the classical "Square Diagram" and the equation relating these three terms is as follows in acetonitrile (Scheme 1.3):

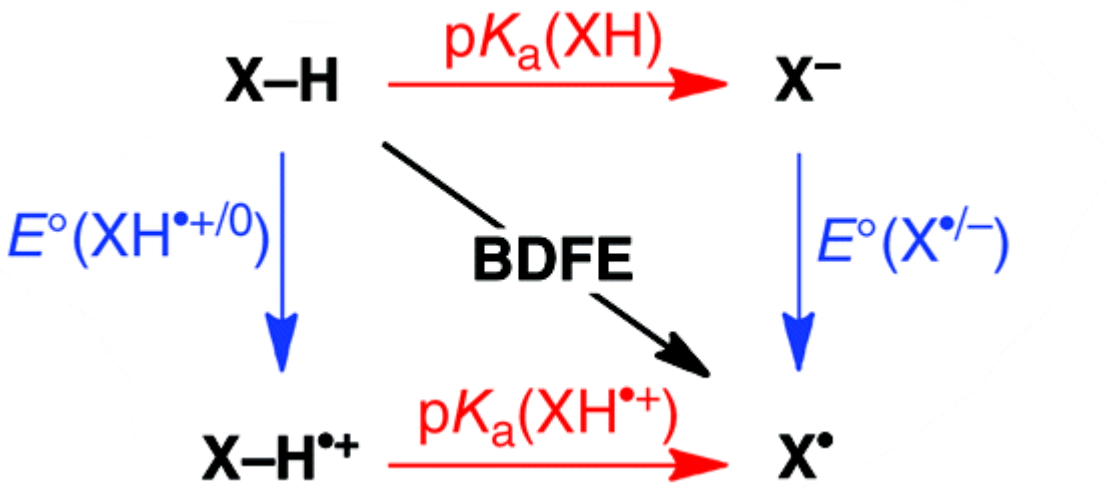

Scheme 1.4. Generic square diagram of HAT and related thermodynamic variables.

Cyclic voltammetry (CV) is a very time- and effort-efficient method of determining redox potentials and related information, and it is a technique used in many chemistry fields as well as materials science, cell biology, and electrical engineering, among others.[11] Differing voltages are

applied through a working and counter electrode to a solution over time according to a set sweep rate of voltage per time, and the amount of current that passes through the solution is then measured. Currents may be oxidative and show as a positive value or reductive and show up as a negative value. A third electrode is used as a reference with a known voltage at which a reversible redox event occurs. However, the reference may drift depending on the solution components, and so often the reference electrode is called a "pseudoreference". Therefore, an additional reference solute may be placed in solution—such as bis-cyclopentadienyl iron(II), or ferrocene, the structure of which is shown below in Figure 1.2.

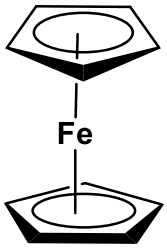

Figure 1.2. The structure of ferrocene. The two cyclopentadienyl ligands are L_2X type ligands, each having a negative charge along with two pi bonds in resonance, resulting in a formal oxidation state of Fe(II). Ferrocene can be reversibly oxidized to ferrocenium, with Fe(III), in solution under most conditions.

Ferrocene undergoes a reversible oxidation from the +2 oxidation state to the +3 oxidation state, which can be clearly seen in a cyclic voltammogram and is then used as an independent reference as compared to the pseudoreference electrode attached to the potentiostat obtaining the voltammogram. [12-13] When placed in solution alongside another species of interest, the average of the cathodic and anodic peak of ferrocene can be set as a "0 V" reference so any reference electrode drift will not interfere with the observations of the voltages at which electrochemical events take place.

In comparison to measuring redox events with CV, it is more difficult to measure pK_a's of acids, particularly in non-aqueous solution where the "pH" scale is completely different than in water. Electrochemical catalysis is often done in non-aqueous environments such as acetonitrile (ACN) or N,N-dimethylformamide (DMF), and while there are reported values for the pKa of acids, they are challenging to measure accurately.[14-17] Although computational methods to determine pK_a's are becoming more commonplace, finding an accurate and precise value computationally may be expensive in terms of computational power. Knowing pK_a values can be important in situations dealing with designing experiments with species, intermediates, or products that are sensitive to pH—and calculations by a non-expert may not provide the accuracy or nuance required for what is needed.[18]

Rhenium complexes of diimine ligands such as 2,2'-bipyridine have been shown to be effective electrocatalysts for CO_2 reduction to CO.[19,20] Various modifications to the diimine ligand have shown changes in the catalyst selectivity and efficiencies. The *fac*-Re(PyBimH)$(CO)_3$Cl (PyBimH = 2-(2-pyridyl)benzimidazole) (**1**) system is particularly interesting because it has an acidic NH group which are often good at promoting catalysis.[21] Experimentally, **1** was found to not be active for CO_2 reduction, whereas when the H was replaced with an alkyl group, it was active. Therefore, we wanted to better understand the acidity and reactivity of the N-H in this system using CV and spectroscopic methods.[22] The structure of **1** is shown in Figure 1.3.

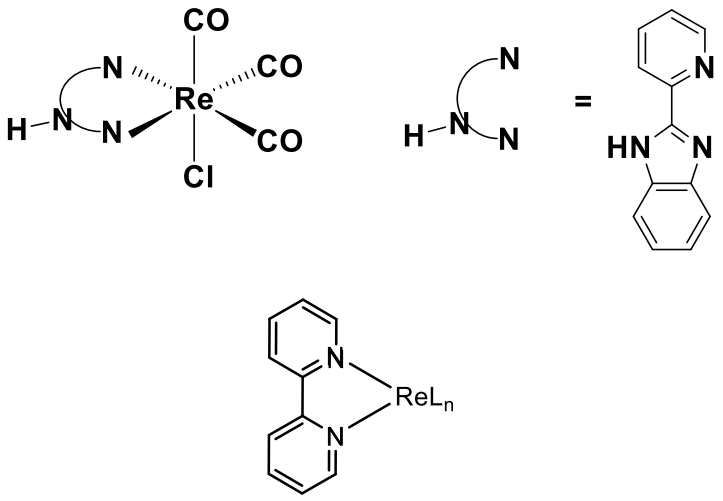

Figure 1.3. The structure of *fac*-Re(PyBimH)$(CO)_3$Cl (**1**) (top) compared to a generic rhenium-bipyridine complex (bottom).

In our investigations of the electrochemical behavior of **1** in acetonitrile, we developed a method for rapidly estimating pKa of acids in acetonitrile using CV. We also determined that upon reduction, **1** loses the N-H via HAT, forming a deprotonated species that cannot be further reduced easily, explaining its failure to catalyze CO_2 reduction. Our results are described below.

1.2. Results

1.2.1. Initial Cyclic Voltammograms

The Re(pybimH)$(CO)_3$Cl complex **1** was synthesized according to reported methods and infrared (IR) and nuclear magnetic resonance (NMR) data matched literature values.[22] Cyclic voltammograms of the complex in acetonitrile with 0.1 M tetrabutylammonium hexafluorophosphate (TBAH) as the electrolyte under Ar were collected using glassy carbon or platinum as the working electrode. In the literature, reduction events were observed at approximately -1.75 V referenced to ferrocenium/ferrocene at a glassy carbon electrode. At both

electrodes, the electrochemical process was irreversible, indicating a rapid chemical reaction after addition of an electron.[22] Notably, the first reduction of *fac*-Re(bpy)$(CO)_3Cl$ is generally reversible due to the ability of the bipyridine ligand to reversibly accept an electron into the π^* orbital of the ligand. A comparison of cyclic voltammograms obtained using a platinum working electrode to a glassy carbon working electrode is shown in Figure 1.4.

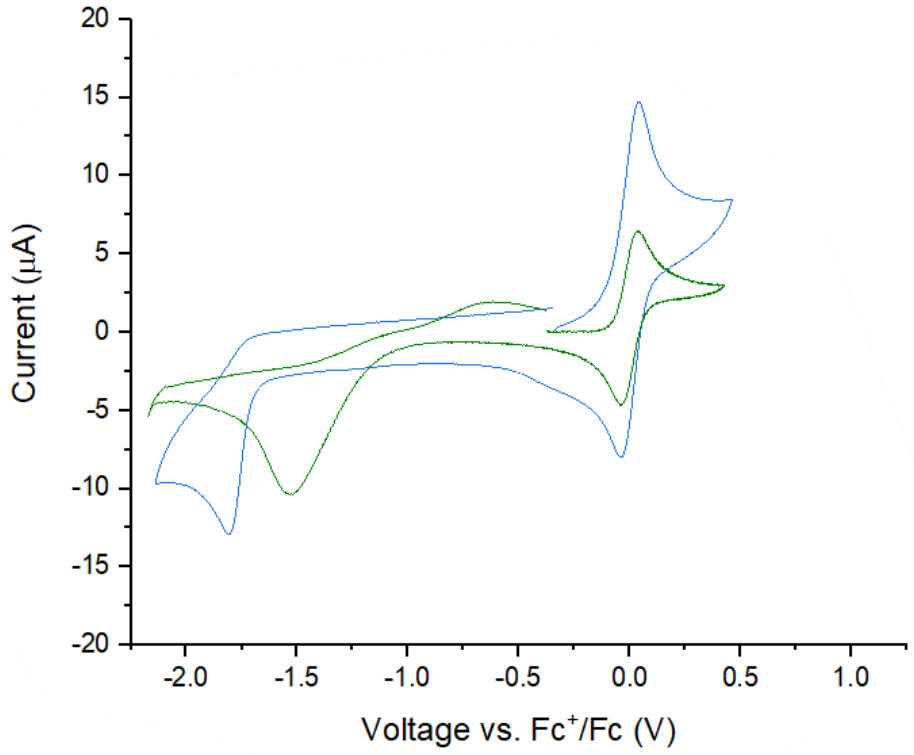

Figure 1.4. Representative cyclic voltammograms of **1** referenced to ferrocene. Samples were dissolved in acetonitrile with 0.1 M TBAH as a supporting electrolyte, and the solutions were sparged with Ar. The only difference between the two scans is that a glassy carbon (blue) was used in one CV and a platinum (green) working electrode was used in the other. The irreversible reduction peak present in both voltammograms is shifted to a more negative potential when a glassy carbon working electrode is used compared to a platinum working electrode.

When cyclic voltammograms were obtained using a platinum working electrode, a reductive peak present with both electrodes was shifted anodically by approximately 0.2-0.3 V as

compared to scans obtained using a glassy carbon working electrode and a small oxidative peak appeared as the applied voltage moved in the positive direction back towards zero.

1.2.2. Scan Rate Study and Mechanistic Consequences

A series of cyclic voltammograms at differing scan rates was obtained to gain information about the reductive electrochemical process at the platinum working electrode (Figure 1.5).

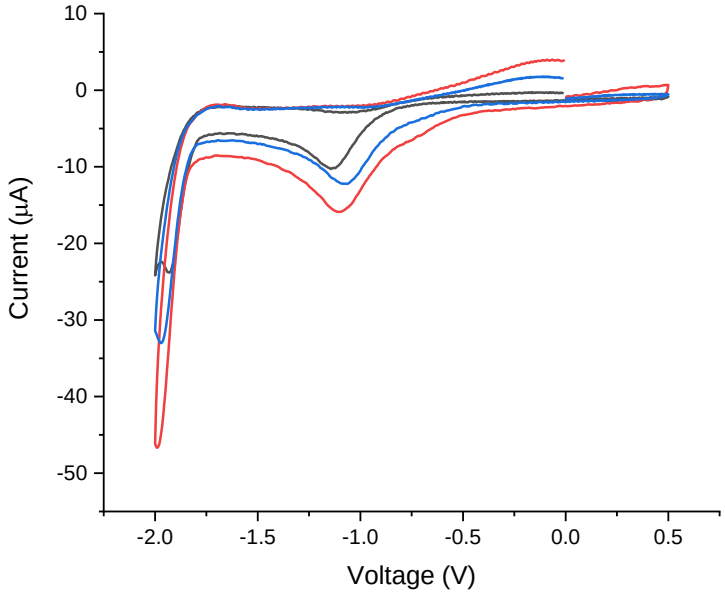

Figure 1.5. Scan rate study of **1** in acetonitrile at a platinum working electrode. Samples were dissolved in acetonitrile with TBAH as a supporting electrolyte. Scans were obtained at 250 mV/s (black), 500 mV/s (blue), and 1000 mV/s (red). As scan rate increases, the magnitude of the peak current increased.

The peak height of the reductive event is observed to increase as a function of scan rate, but the exact relationship between scan rate and peak height provides mechanistic information about the electrochemical changes that are taking place. When there is a linear relationship between the square root of the scan rate and the peak height, the reaction taking place is diffusion-controlled, while a linear relationship between the unmodified scan rate and the peak height

suggests that a reaction is taking place at the electrode's surface; in the context of this study, a HAT reaction between the N-H bond in PyBimH and the platinum electrode surface would be supported by a linear relationship between scan rate and peak height but not peak height and the square root of the scan rate.[23] The relationship between the scan rate and square root of scan rate were correlated to peak height (Figure 1.6).

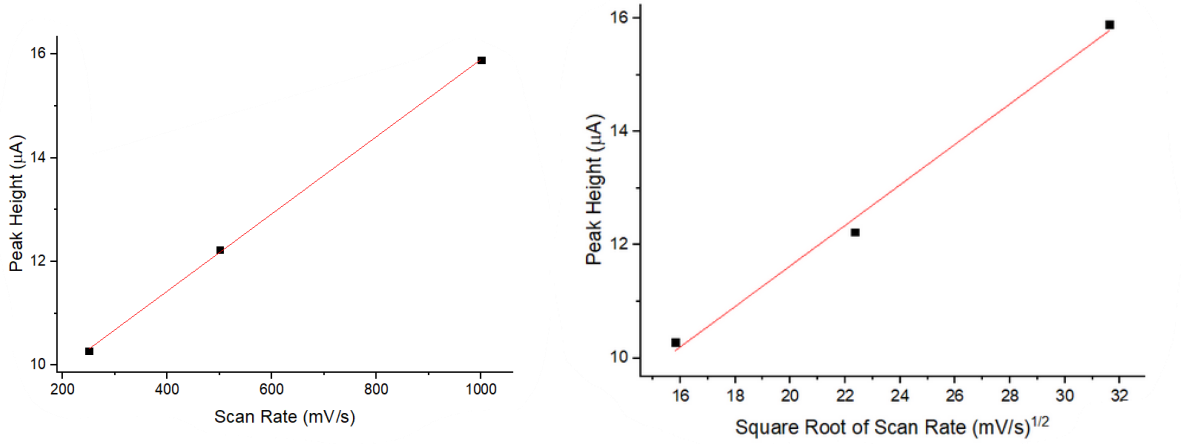

Figure 1.6. Relative peak height versus scan rate or square root of scan rate of **1** in acetonitrile at a platinum electrode. The fit using the unmodified scan rate is given by $\text{Peak Height}\,(\mu\text{A}) = \left((7.5 \pm 0.1) \times 10^{-3}\,\frac{\mu\text{A}\cdot\text{s}}{\text{mV}}\right)\left(\text{Scan Rate}\,\left(\frac{\text{mV}}{\text{s}}\right)\right) + \left((8.45 \pm 0.08) \times 10^{-2}\ \text{A}\right)$, with a value of $R^2 = 0.99975$. The fit using the square root of the scan rate is given by $\text{Peak Height}\,(\mu\text{A}) = \left((3.5 \pm 0.3) \times 10^{-2}\,\frac{\mu\text{A}\cdot\sqrt{\text{s}}}{\sqrt{\text{mV}}}\right)\left(\sqrt{\text{Scan Rate}}\,\left(\frac{\text{mV}}{\text{s}}\right)^{\frac{1}{2}}\right) + (4.5 \pm 0.7\ \mu\text{A})$, with a value of $R^2 = 0.9886$.

Based on comparing R^2 values between the calculated fits, the peak height showed a stronger correlation to the scan rate compared to the square root of the scan rate, leading to the conclusion that the electrochemical reaction is happening at the electrode surface. This surface-related reduction could be due to PCET of the N-H to the platinum electrode, with an electron forming a Pt-H species on the surface (Scheme 1.4).

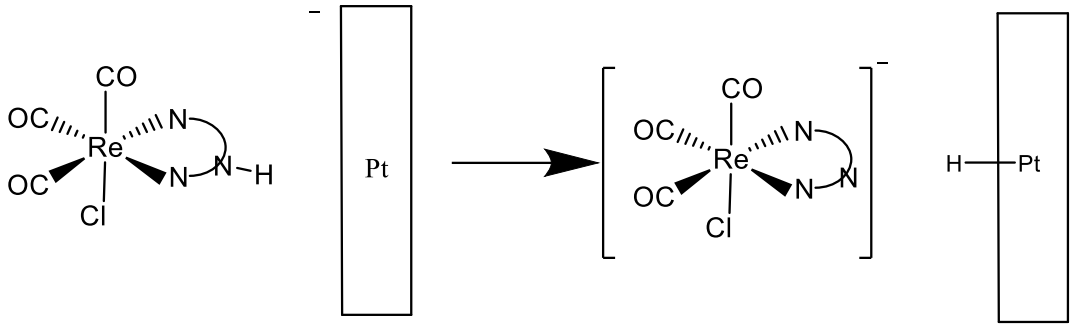

Scheme 1.4. Proposed PCET reaction occurring at a platinum electrode surface.

To explore the reason for the difference in reduction potentials between using a glassy carbon and platinum working electrode, a scan rate study of **1** under glassy carbon was also used to determine if there was a difference in the reaction mechanism between the two types of electrodes. Example voltammograms of the scan rate study are shown in Figure 1.7.

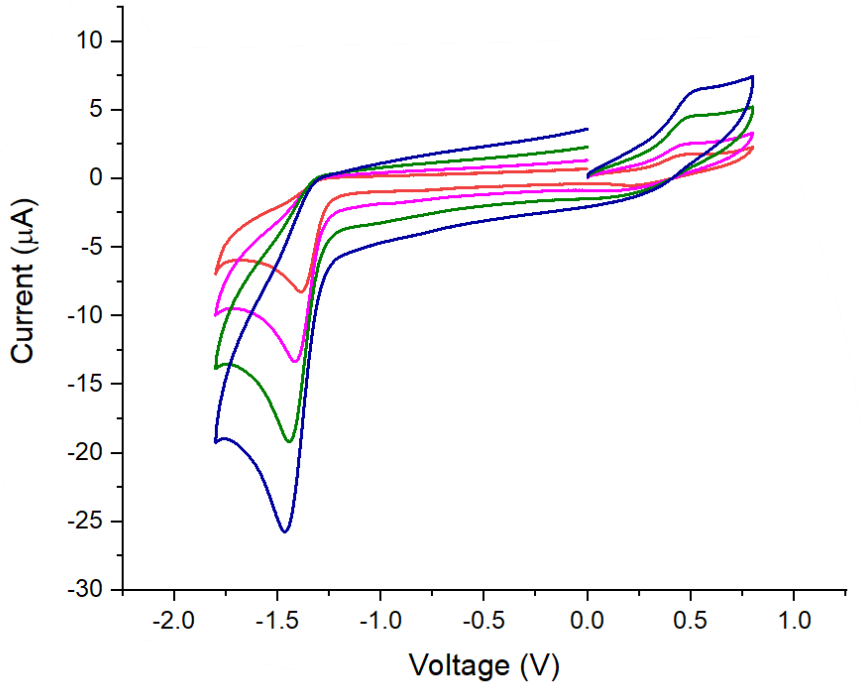

Figure 1.7. Scan rate study of **1** in acetonitrile at a glassy carbon working electrode. Samples were dissolved in acetonitrile with TBAH as a supporting electrolyte. Scans were obtained at 100 mV/s (red), 250 mV/s (purple), 500 mV/s (green), and 1000 mV/s (blue).

The peak height is again qualitatively observed to increase with respect to scan rate, but if there is a different relationship between scan rate and peak height when comparing different working electrodes, then a difference in the mechanism of reduction would be confirmed. Peak height plotted as a function of both scan rate and the square root of scan rate is shown in Figure 1.8.

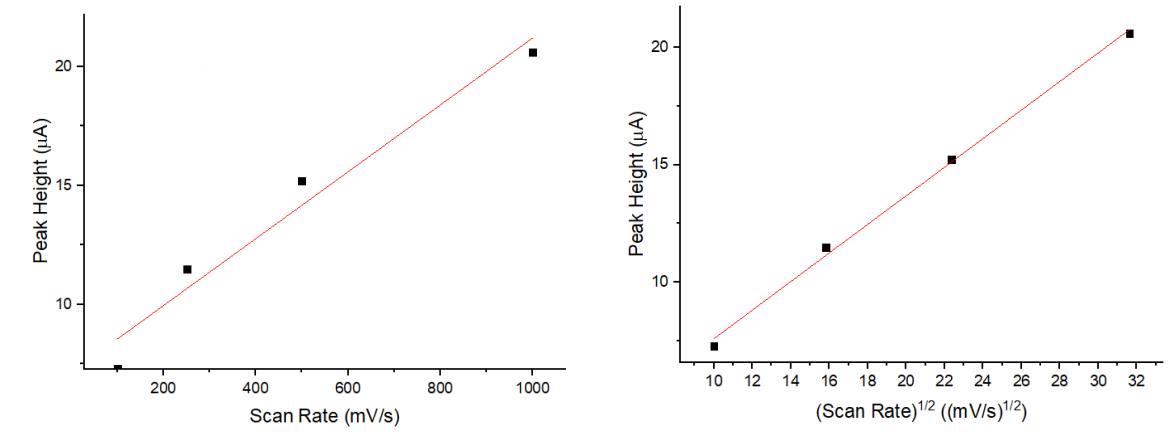

Figure 1.8. Relative peak height versus scan rate or square root of scan rate of **1** in acetonitrile at a glassy carbon electrode. The fit using the unmodified scan rate is given by $\text{Peak Height } (\mu\text{A}) = \left((7.5 \pm 0.1) \times 10^{-3} \frac{\mu\text{A}\cdot\text{s}}{\text{mV}}\right)\left(\text{Scan Rate } \left(\frac{\text{mV}}{\text{s}}\right)\right) + (7 \pm 1\ \mu\text{A})$, with an R^2 value of 0.94199. The fit using the square root of the scan rate is given by $\text{Peak Height } (\mu\text{A}) = \left((6.1 \pm 0.2) \times 10^{-1} \frac{\mu\text{A}\cdot\sqrt{\text{s}}}{\sqrt{\text{mV}}}\right)\left(\sqrt{\text{Scan Rate}}\ \left(\frac{\text{mV}}{\text{s}}\right)^{\frac{1}{2}}\right) + (1.5 \pm 0.5\ \mu\text{A})$, with an R^2 value of 0.99608.

From R^2 values, the peak height shows a stronger correlation to the square root of the scan rate than the scan rate, which is the opposite of the result obtained from using a platinum electrode. This means that the chemical change **1** undergoes is in solution and not while adsorbed to the electrode. Although a different mechanism is taking place when at a glassy carbon working electrode, it is possible that PCET or another reaction taking place at the NH group is taking place similar to the overall reaction taking place at platinum. compared to platinum, further supporting

a PCET reaction occurring when using a platinum electrode as the corresponding reaction at glassy carbon is not at the electrode surface.

1.2.3. Investigation of PCET Activity of Benchmark Acids at a Platinum Electrode

It is known that acids can be directly reduced at electrodes, and that platinum electrodes in water show a reduction potential that is related to pKa.[24] The reduction of aqueous acids such as pyridinium at platinum was originally incorrectly ascribed to formation of pyridinyl radical, but is actually PCET involving transfer of a proton from the acid to the Pt surface and transfer of an electron to form a surface-bound Pt-H that rapidly forms hydrogen.[25] Inspired by the pKa-dependence observed at a Pt electrode in water, and the differing behavior of **1** at platinum as compared to glassy carbon, we set out to investigate the relationship between features observed in cyclic voltammograms and the pKa of acidic protons in acetonitrile. CVs of acetic acid (2.5 mM), anilinium (2.62 mM), benzoic acid (2.87 mM), morpholinium (2.53 mM), piperidinium (2.47 mM), pyridinium (2.51 mM), and trifluoroacetic acid (2.54 mM) were obtained in acetonitrile under Ar. The pKa values of these acids are known in acetonitrile.[14-17] The structures of the selected benchmark acids are shown below in Figure 1.9:

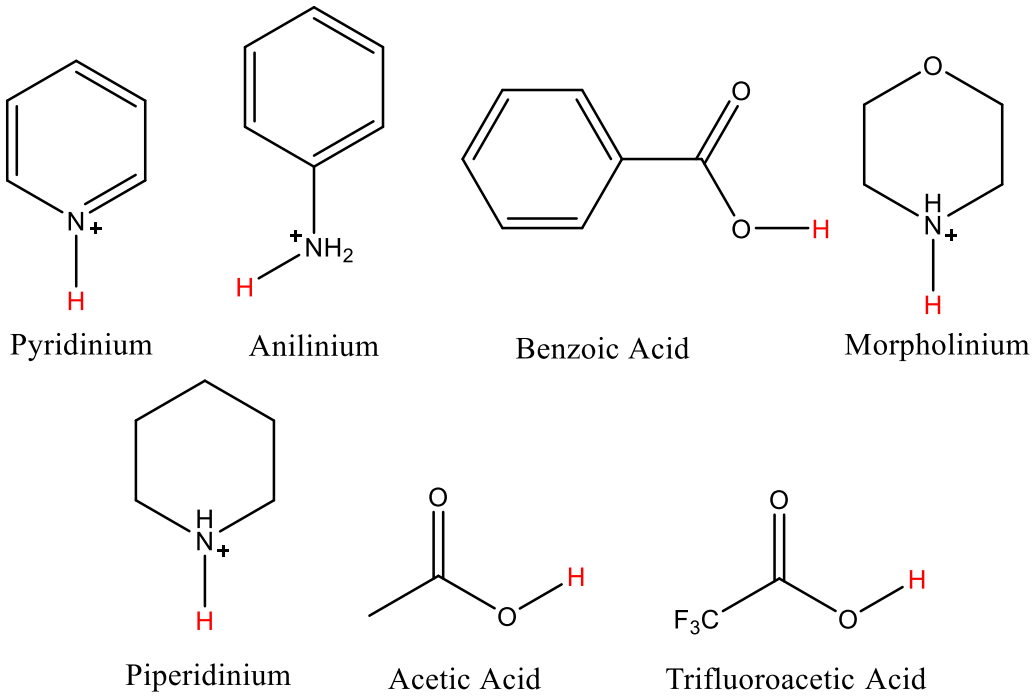

Figure 1.9. Acids examined by CV in acetonitrile at a Pt electrode. Acidic protons are colored red.

Usage of both protonated ammonium N-H bonds and carboxylic acid O-H bonds within the set of benchmark acids ensured that possible bias within the chemical environment that may affect results is not ignored. Cyclic voltammograms of each benchmark acid in acetonitrile showed irreversible reduction events at different voltages, evidenced by an observed reductive current with no oxidative current as voltage returned towards 0 V. The irreversible nature of these events indicates that upon reduction, a fast chemical step follows. These CVs were obtained in the presence of Fc to reference the reduction events (Figure 1.10).

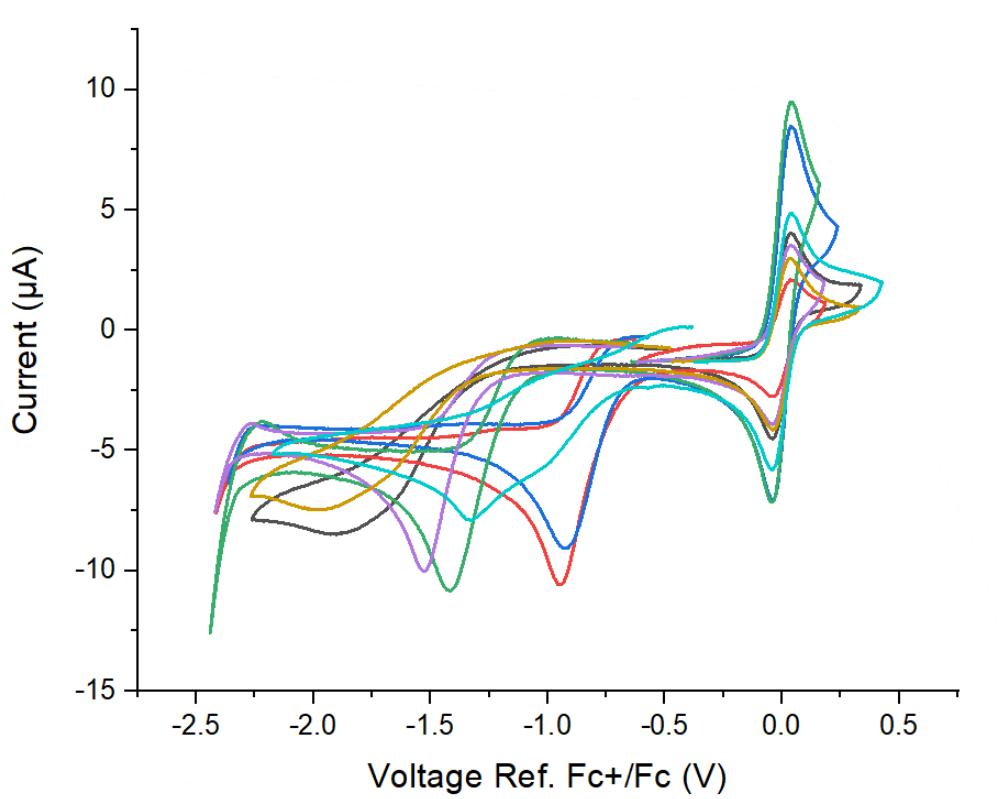

Figure 1.10. Representative cyclic voltammograms for various benchmark acids referenced to ferrocene. Samples were dissolved in acetonitrile with TBAH as a supporting electrolyte. The benchmark acids shown are benzoic acid (black), pyridinium (red), anilinium (blue), morpholinium (green), piperidinium (purple), trifluoroacetic acid (teal) and acetic acid (orange). Voltammograms were adjusted so that the $E_{1/2}$ value of ferrocene was placed at 0 V as a reference.

Once the CVs were adjusted so the $E_{1/2}$ point of the ferrocene oxidation/reduction was at 0 V, comparing the voltages at which the benchmark acids is possible. The scans of each acid look like they have different maximum and minimum voltages due to the adjustment of the ferrocene $E_{1/2}$ location, which arises from voltaic drift of the silver reference electrode used with the hardware. Notably, the reduction potentials of these acids were much more positive than those reported at glassy carbon electrodes in acetonitrile.[24, 26] The literature pK_a values of the benchmark acids were compared to average peak location referenced to ferrocene over 2-4 runs (Table 1.1).

Table 1.1. Benchmark acid/base pK_a values and averaged peak reductive current potential.

Compound	pK_a in Acetonitrile	Averaged Peak Current Potentail (V)
Acetic acid	23.51	-1.983 ± 0.005
Anilinium hydrochloride	10.64	-0.92 ± 0.01
Benzoic acid	21.51	-1.93 ± 0.01
Morpholinium hydrochloride	16.61	-1.418 ± 0.003
Piperidinium hydrochloride	19.35	-1.51 ± 0.01
Pyridinium hydrochloride	12.53	-0.96 ± 0.01
Trifluoroacetic acid	12.65	-1.36 ± 0.05

The peaks showed a trend that was then examined quantitatively to yield a relationship between average peak location and pK_a illustrated in Figure 1.11.

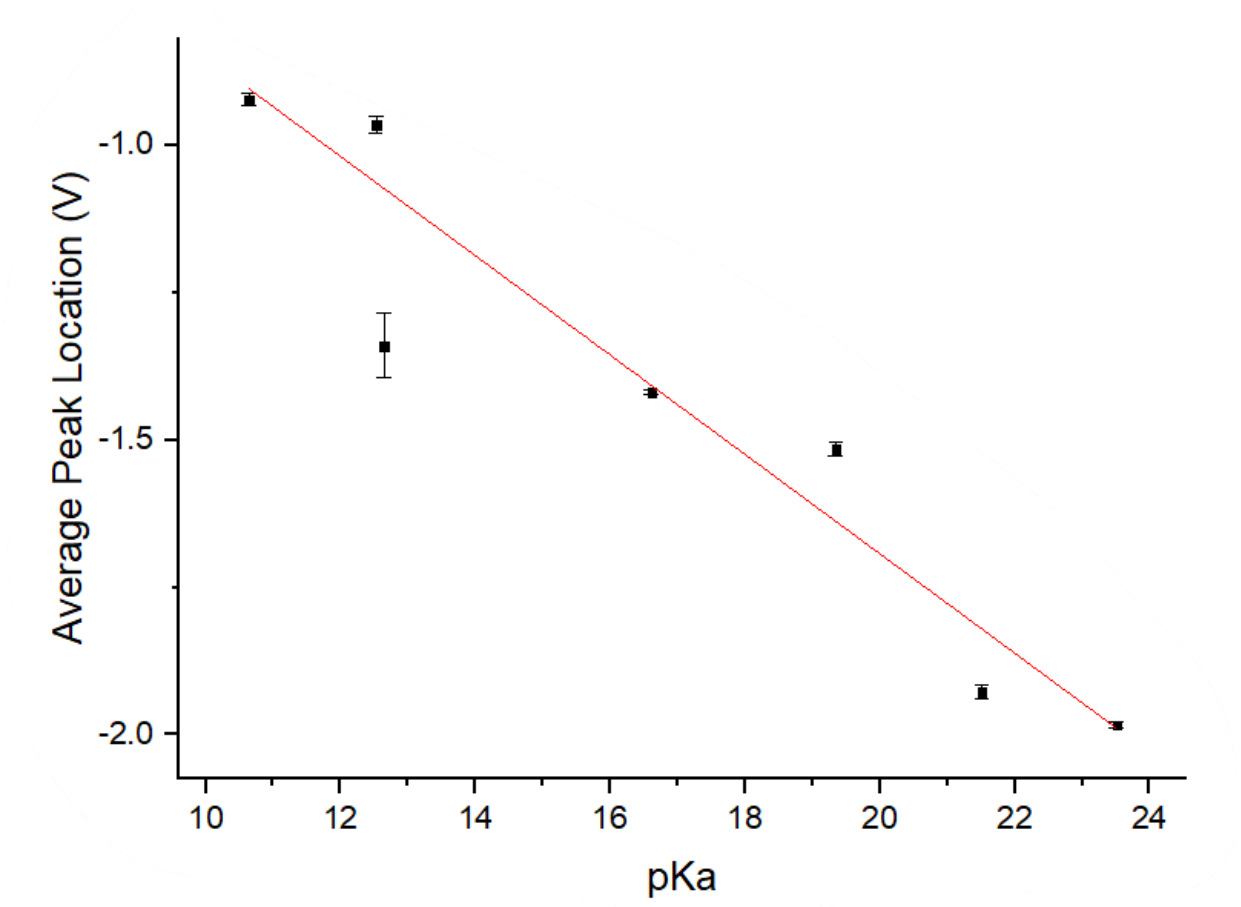

Figure 1.11. Reduction peak voltage versus pK_a for benchmark acids. The best fit equation is given by $\text{Peak Location (V)} = (-0.084 \pm 0.005\ \text{V})(pK_a) + (0.0 \pm 0.1\ \text{V})$, with an R^2 value of 0.97594.

An initial impression of the trend of an anticorrelation between peak location and pK_a is that the trend seems reasonable; a more negative voltage required to cause a reduction at the acidic X-H bond would logically correlate with a stronger bond or higher pK_a. Because the reductions are irreversible, using peak locations is problematic for finding the formal half reaction voltage, $E_{1/2}$, which is normally found by averaging the location of the reduction and oxidation peaks in a reversible redox event. Voltage at half the height of the peak current compared to an estimated baseline has been used to estimate $E_{1/2}$ for irreversible processes.[27] Therefore, a second plot relating the pK$_a$ to the voltage at half peak height was constructed (Figure 1.12).

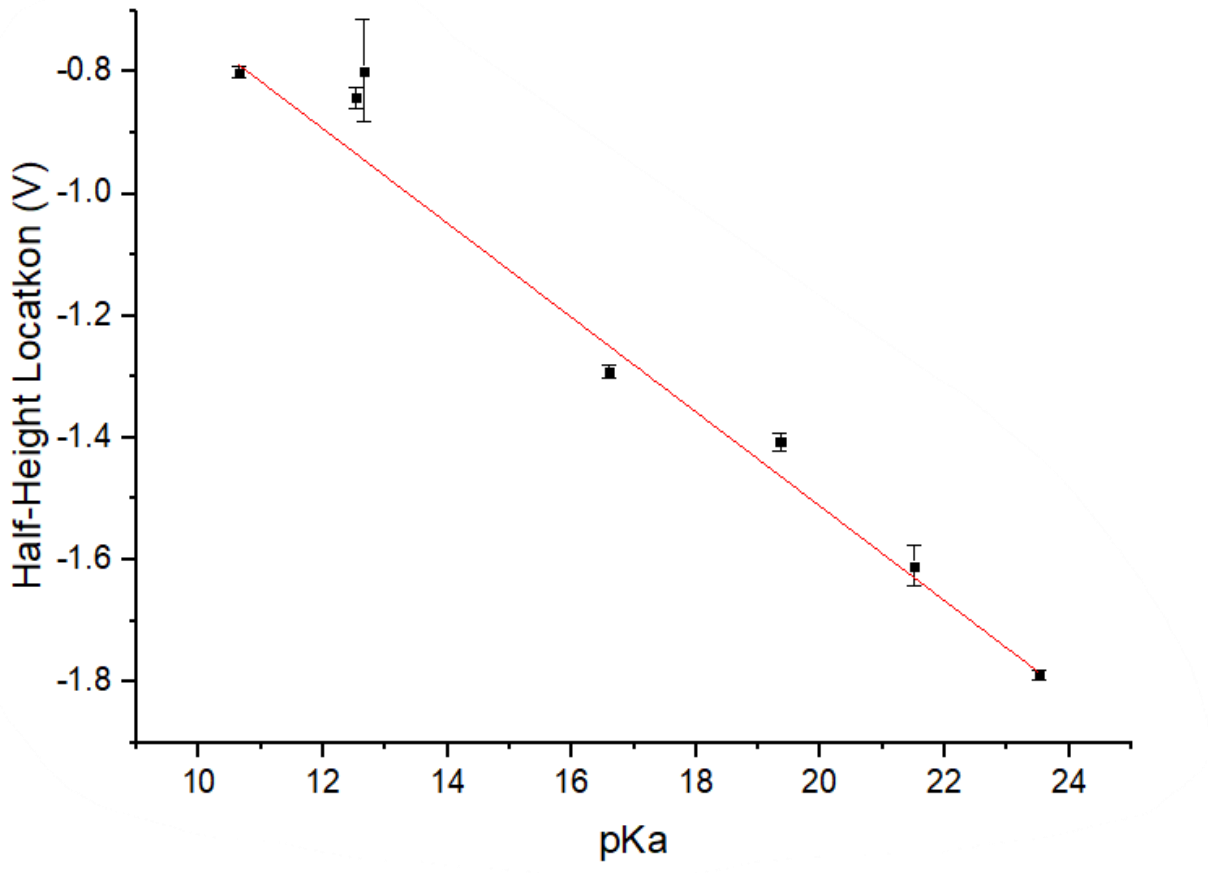

Figure 1.12. Voltage at half peak height versus pK$_a$. The line of best fit is given by $\left(\text{Half} - \text{Height Location (V)}\right) = (-0.077 \pm 0.003\ \text{V})(\text{p}K_a) + (0.03 \pm 0.06\ \text{V})$, with an R^2 value of 0.98856.

From the R^2 value, the peak at half height gives a stronger correlation to the pK_a than the peak location; however, literature gives ways to estimate $E_{1/2}$ through more consistent mathematical estimations.[27] An analysis using the inflection point of the peak as a measure of the voltage at half-peak height was then undertaken, shown in Figure 1.13.

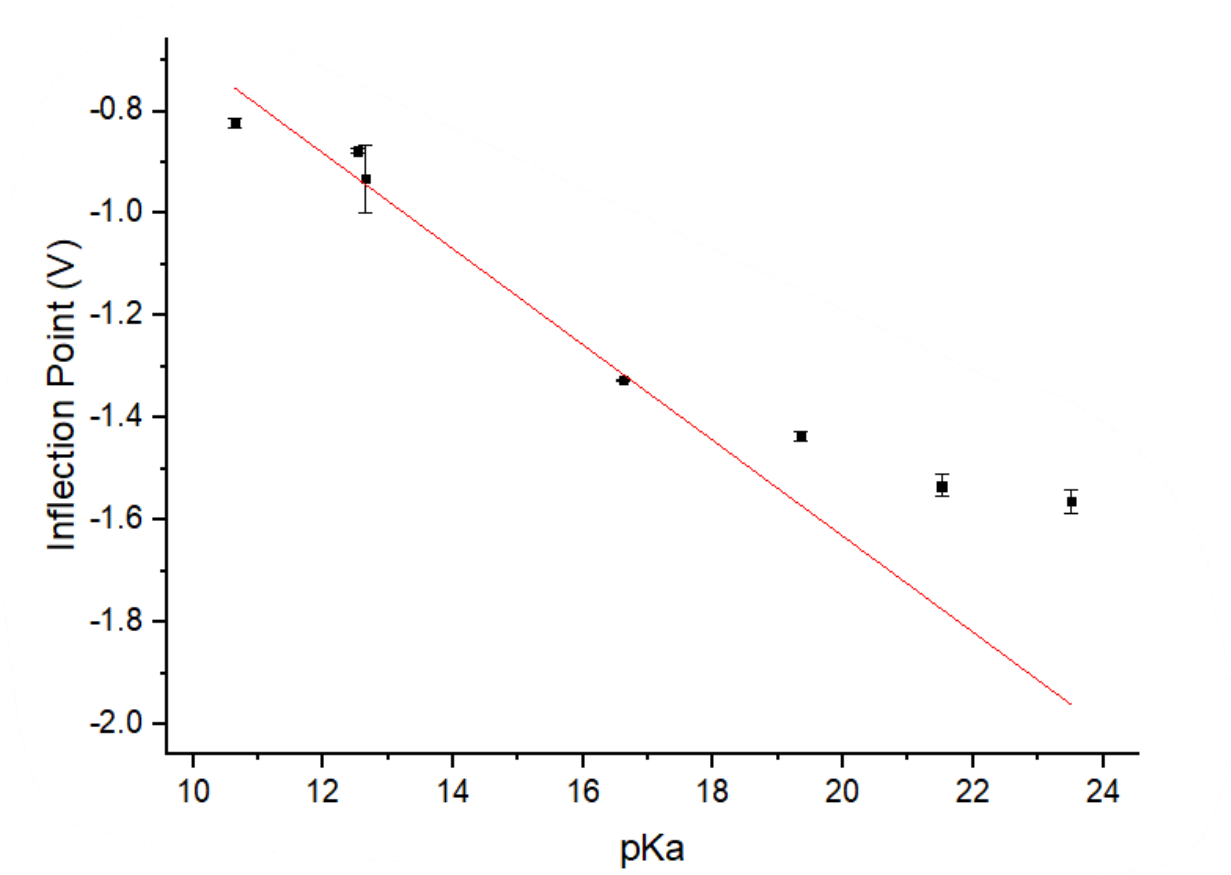

Figure 1.13. Inflection point voltage as a function of pK_a. The line of best fit is given by $\text{Inflection Point (V)} = (-0.09 \pm 0.01\ \text{V})(pK_a) + (0.2 \pm 0.2\ \text{V})$, with an R^2 value of 0.93221.

The reason for the discrepancy in uncertainty between trifluoroacetic acid and the other tested acids is not known, but could be due to rapid proton reduction at the electrode. Of the three fits, the peak at half height from an estimated baseline gave the strongest correlation between determined voltage and pK_a as shown by the R^2 values. Using the location of the half height of the

peak, the predicted pK_a of **1** in acetonitrile was interpolated as 20 ± 1, close to piperidinium in acetonitrile.

1.2.4. IR Spectra of Re(pybimH)(CO)$_3$Cl and Related Species

For further confirmation of the HAT event taking place at the N-H in **1**, deprotonation via a base was compared to the effects of reductive voltage. To that end, IR spectra were obtained for **1** in the absence and presence of triethylamine, which has a pK_a of 18.82 in acetonitrile, lower than the predicted pK_a of **1** (Figure 1.14).[17]

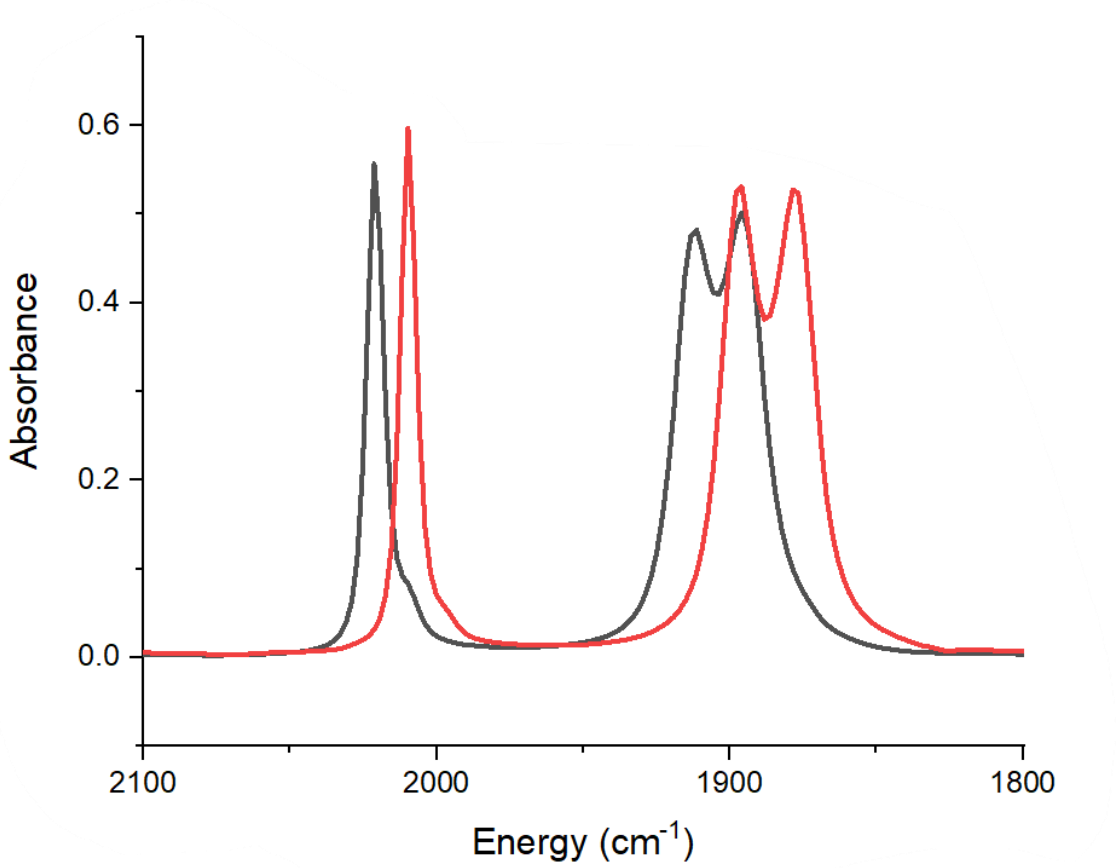

Figure 1.14. IR spectrum of **1** in acetonitrile in the absence and presence of base. The carbonyl stretching (1800-2100 cm^{-1}) and N-H stretching (3100-3200 cm^{-1}) regions are shown for samples of **1** (black) and **1** in the presence of triethylamine (red). In the sample with added triethylamine, the N-H stretching peak is reduced in size and the carbonyl peaks shift to a lower wavenumber.

After adding a qualitative amount of triethylamine, a slight shift in the peaks around 1800 and 2000 cm^{-1} as well as the partial disappearance of a peak near 3164 cm^{-1} suggests partial deprotonation. A study using differing amounts of triethylamine was not pursued, but addition of imidazole instead of triethylamine resulted in a spectrum with heights and locations between the two shown. Partial deprotonation is a reasonable conclusion because although **1** is predicted to be more basic than triethylamine, an appreciable equilibrium between protonated and deprotonated **1** would still be established through adding a super-stoichiometric amount of triethylamine.

A series of infrared spectroelectrochemistry (IR-SEC) spectra were obtained to observe changes in solution that occur while applying reducing voltage to **1** at a Pt mesh electrode. IR-SEC involves obtaining an IR spectrum while applying a voltage to the solution-phase sample contained within the cell. Through applying a voltage, various reactants, products, and intermediates can all be observed by infrared spectra. Furthermore, changes in chemical species can be detected live as individual infrared signals are monitored over the course of spectra obtained at a variety of applied voltages.[28] IR-SEC spectra in the carbonyl region are shown in Figure 1.15.

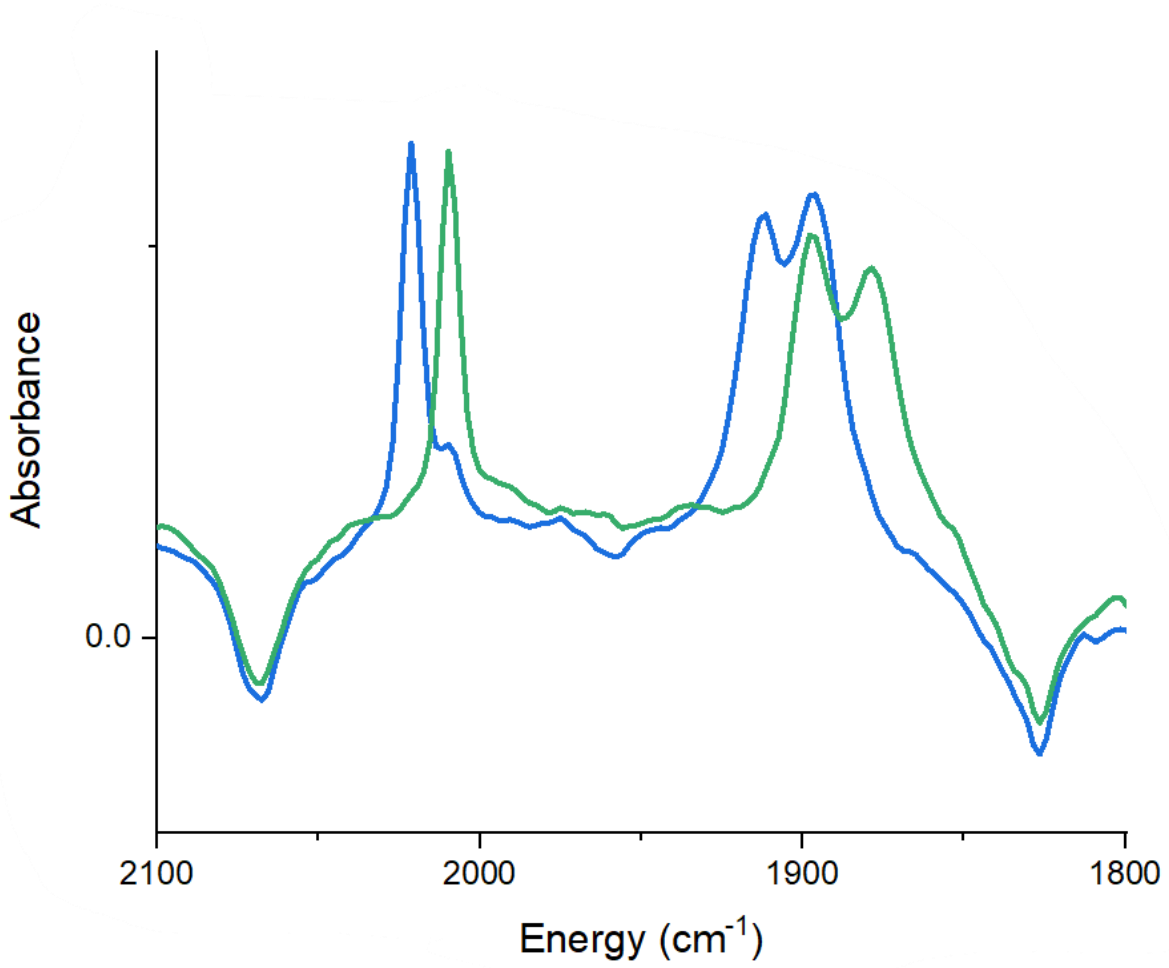

Figure 1.15. IR-SEC of **1** at differing applied voltages. Samples were dissolved in acetonitrile with TBAH as a supporting electrolyte. The carbonyl stretching region is shown for **1** under application of 0 V (blue) and -2.7 V (green).

The N-H region of the infrared spectra contained too much interference to draw clear conclusions, and so the only clear indicators of deprotonation were from the carbonyl region. From the IR-SEC spectra, several changes were observed upon reduction. The three Re-CO signals shifted to lower wavenumbers, indicating more back-bonding from the Re. The carbonyl IR signals observed upon reaction with trimethylamine were nearly identical to those observed upon reduction in the IR-SEC cell. This would suggest that the two different processes—reaction of the complex with triethylamine and reduction through applied voltage—give the same product, a

deprotonated and monoanionic **1**. A comparison of the carbonyl peak locations is shown in Table 1.2.

Table 1.2. Comparison of carbonyl IR peaks in neutral and reduced **1**.

Peak Location at 0 V (cm^{-1})	Peak Location at -2.7 V (cm^{-1})	Peak Location with TEA (cm^{-1})
2021.2 ± 0.7	2009.7 ± 0.7	2009.7 ± 0.7
1911.3 ± 0.7	1898.8 ± 0.7	1895.9 ± 0.7
1895.9 ± 0.7	1878.5 ± 0.7	1878.5 ± 0.7

The effect of adding triethylamine was the same as applying a reductive voltage, further supporting the deprotonation of the PyBimH ligand during electrochemical reduction at a platinum electrode in the cyclic voltammograms and the IR-SEC.

1.2.5. Computational Studies

Computational studies of the complex were pursued for further understanding of the observed reactivity. The structure of **1** was optimized at the MN-15L/def2-TZVP level, with acetonitrile modeled using the polarized continuum model. The calculations were performed by Dr. Grice, who provided the results discussed below. The HOMO and LUMO of **1** are shown in Figure 1.16.

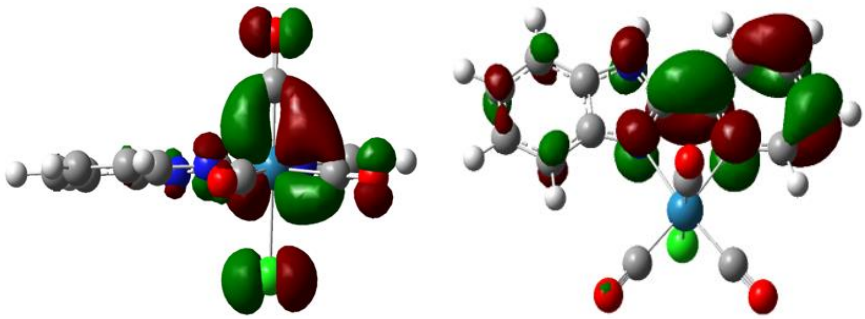

Figure 1.16. Calculated frontier molecular orbitals of protonated **1**. The HOMO (left) and LUMO (right) are shown. The HOMO is metal- and carbonyl-based and the LUMO is primarily ligand π^* in character. The complex is rotated differently in the two images to give the best visualization of the appropriate FMOs.

Reduction events should reasonably transfer electrons to the lowest-energy orbital that can accept an electron. Therefore, the LUMO of **1** indicates that reduction occurs primarily at the ligand, similar to the redox-non-innocent 2,2'-bipyridine ligand in $Re(bpy)(CO)_3Cl$. The molecular orbitals of the deprotonated species are shown in Figure 1.17.

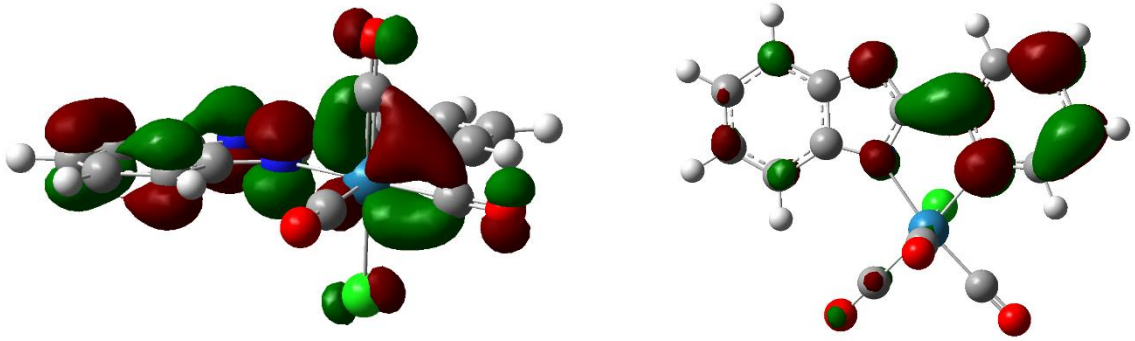

Figure 1.17. Calculated frontier molecular orbtials of deprotonated **1**. The calculated HOMO (left) and LUMO (right) are shown. The LUMO is still π^*, but the HOMO is now both metal- and ligand-based.

To construct a square diagram for a comparison between experimental and computed results, several related species were also optimized. From this, relevant pKa values and reduction

potentials were calculated based on literature approaches.[29] The DFT-calculated pKa was within 2 pKa units of the CV-measured value, showing reasonable agreement with experimental results. Relevant processes and their calculated thermodynamic quantities are shown as a square diagram in Figure 1.18.

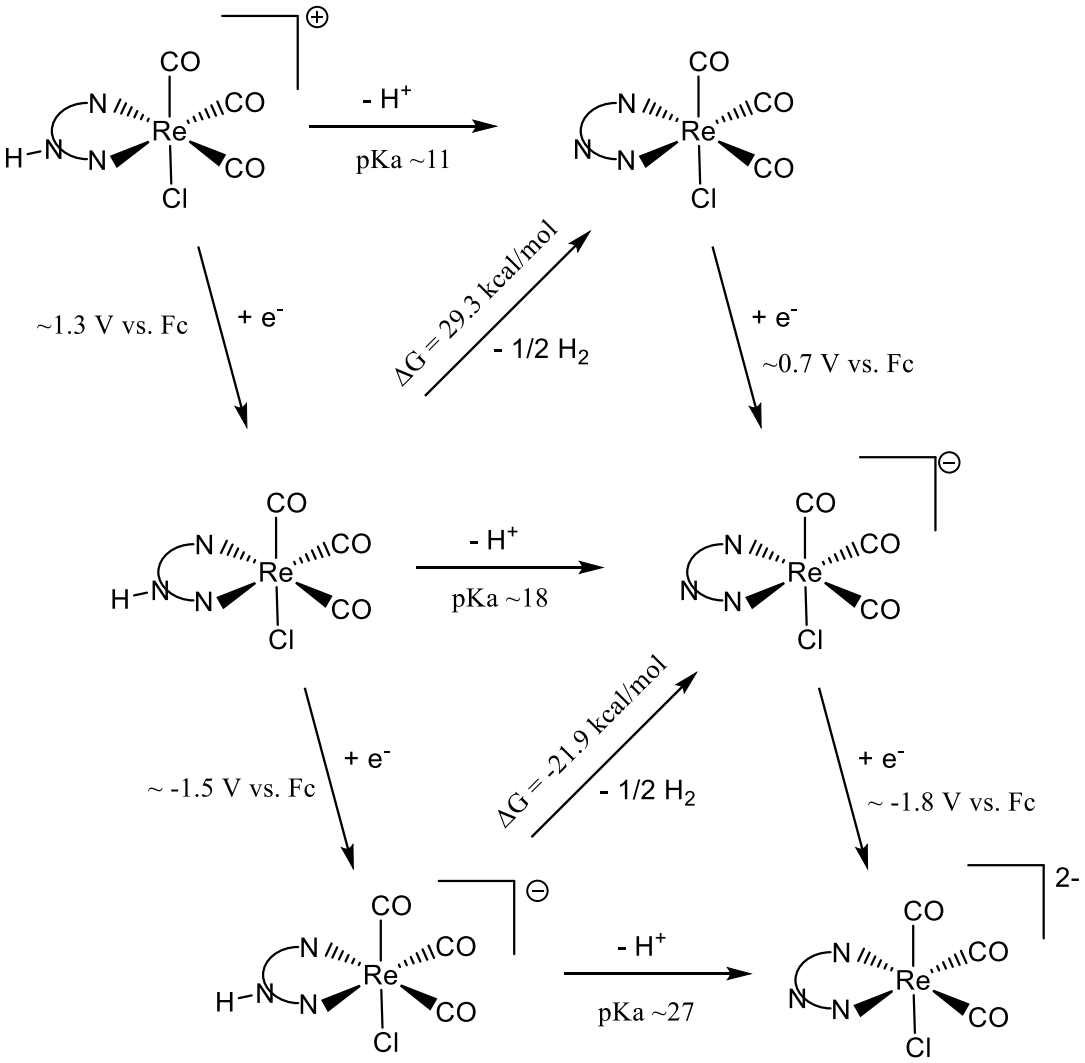

Figure 1.18. PCET diagrams for **1** with calculated thermodynamic quantities. The protonated, singly reduced species shows a favorable deprotonation overall while the unreduced species shows an unfavorable deprotonation.

Calculations of the deprotonation of **1** showed an estimated pK_a of 18, which is in relatively good agreement with the estimate provided by the fit to the benchmark acids. After being reduced, deprotonation of **1** is calculated to have a significantly negative ΔG value, in agreement with the conclusion of a PCET reaction occurring upon reduction. Using the calculated pKa and oxidation potentials, the BDFE of the N-H can be estimated at 95.7 kcal/mol with Equation 1. The BDFE of H_2 in acetonitrile is greater than that of the N-H bond at 102.3 kcal/mol, but a comparison of the values leads to the conclusion that **1** would not spontaneously react to generate H_2, as two N-H's would need to be broken to form one H-H. This is also consistent with DFT-calculated reaction energy to form H_2 from **1**. Upon reduction, **1** forms an anion that is much less acidic (pKa = 27) than **1**. Using this value and the calculated oxidation potential of $[Re(pybim)(CO)_3Cl]^{2-}$, the N-H BDE is only 50.4 kcal/mol, making H_2 production favorable from PCET. Therefore, even at a glassy carbon electrode, the reduction of **1** would result in H_2 formation and a formal deprotonation rather than an overall reduction event.

The calculated reduction potential of deprotonated **1** is also further negative than reduction of **1**. This would only be the first reduction of the Re(pybim) species, and it is well known that catalysis from Re(bpy) and related compounds only occurs after accepting two electrons. This explains why CO_2 reduction wasn't observed. The first reduction is actually a deprotonation event, and thus catalysis wouldn't be expected to occur until after the "third" reduction event, which occurs at a much more negative potential and therefore requiring a much larger overpotential.

1.3. Conclusions

An investigation into the electrochemical properties of the rhenium complex *fac*-$Re(PyBimH)(CO)_3Cl$ led to the discovery that reduction at a platinum electrode in acetonitrile is actually a deprotonation HAT event, which instigated an investigation into the measurement of X-

H bond dissociation energies through electrochemistry. A time- and effort-efficient method of estimating the pK_a values of acids in acetonitrile through CV using a platinum electrode was explored and proven effective. A model was first constructed using benchmark acids with known pK_a values in acetonitrile. A clear trend emerged from the benchmark acids chosen except for trifluoroacetic acid (TFA) for unclear reasons; one possibility is that TFA protonates acetonitrile and so cyclic voltammetry of a solution instead becomes a measurement of the pKa of protonated acetonitrile. The model was extrapolated to an unexplored acidic N—H bond in **1**, and the results of the model agreed to within a couple pK_a units of DFT calculations. The importance of the identity of the electrode was discovered as using a glassy carbon electrode did not show the same proton reduction activity. To improve understanding of the trend, further experiments with other acidic species could give a more accurate trend or even result in the discovery of why some species are exceptions. Experimentation with different systems of electrodes could also give information about the capabilities, limitations, and extent of this method in case a reaction or electrochemical setup requires one type of electrode over another.

Chapter 2. Organic Molecules as Electrocatalysts in the Reduction of Carbon Dioxide

2.1. Introduction

2.1.1. Carbon Dioxide Reduction

Climate change is being driven by CO_2 in the atmosphere both because of the vast amounts of CO_2 produced by human activity and because of its present abundance in the atmosphere compared to other greenhouse gases.[30] As discussed in chapter 1**,** carbon dioxide reduction is an important process that constitutes the reductive half of artificial photosynthesis. A wide variety of

homogeneous and heterogeneous metal complexes have been applied to this reaction, but they often suffer from several drawbacks, including stability, selectivity, efficiency, environmental, toxicological, and cost issues. If a catalyst is to be scaled up to industrial use, it needs to be relatively inexpensive. Currently, many effective CO_2-reducing catalysts use iridium, rhenium, ruthenium, and other rare metals.[31]

Simple organic molecules would be the ideal homogenous catalyst as they can be much cheaper than metal catalysts and easier to produce on larger scales. However, organic catalysts for CO_2 reduction or similar reactions are relatively rare, but not unknown. Saveant and co-workers found that benzonitrile and simple benzoate esters were catalysts for CO_2 reduction, albeit at very negative potentials—further negative than most metal catalysts.[32] The more negative the potential that a catalyst operates, the more power is needed to drive catalysis overall, even if the change in free energy is not demanding. Therefore, catalysts that can operate at more positive potentials (but still negative compared to ferrocene) are desirable. A key balance is needed between finding a molecule that can be reduced and one that is nucleophilic enough once reduced to react with CO_2. In order to identify catalysts with more positive catalytic potentials, we examined other redox-active organic molecules in the literature.

2.1.2. Introduction to Buckminsterfullerene

Buckminsterfullerene has been shown to catalytically reduce dinitrogen to ammonia in water.[33] Due to its large, conjugated π system, it can reversibly be reduced multiple times, opening the door for the possibility of activity as a catalyst for the reduction of carbon dioxide. The molecular structure of buckminsterfullerene, or C_{60}, is shown below in Figure 2.1.

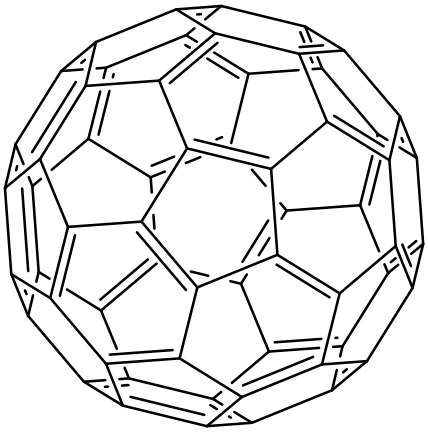

Figure 2.1. The structure of buckminsterfullerene, C_{60}.

The various electrochemically reduced states of C_{60} have been studied by Kalsbeck with substrates like H_2O and O_2, but the reduced species up to the dianion was reported not to react with carbon dioxide.[34] Besides this report, there have currently been no studies testing for CO_2 reduction catalysis, which further encourages an investigation into its potential as an electrocatalyst. A review by Kroto, Allaf, and Balm reports that C_{60} catalyzes the formation of singlet oxygen and can form adducts with some inorganic complexes and metals, but is relatively unreactive beyond that.[35] In this study, the reactivity of C_{60} as an electrocatalyst is explored, showing an appreciable activity in 1,2-dichlorobenzene under an atmosphere of carbon dioxide.

2.1.3. Introduction to Benzil

Benzil has been explored for its electrochemical properties in nonaqueous solvents (acetonitrile and dimethylformamide) and water containing a variety of metal cations.[36-38] The structure of benzil is shown below in Figure 2.2.

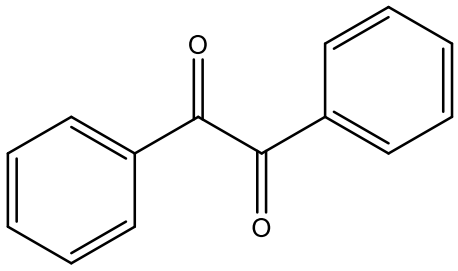

Figure 2.2. The structure of benzil.

Two reversible reductions are observed when cyclic voltammograms of benzil are obtained in an ionic liquid, the second of which becomes irreversible in the presence of acetonitrile due to protonation of the dianion by an adventitious proton source.[37] According to two reports, benzil shows good electrocatalytic activity with carbon dioxide; another source shows greater activity with a combination of benzil and pyridine in solution.[39,40] Benzil is attractive as an electrocatalyst because it is commercially available, quite cheap at $51.89 for 250 g ($0.2076 per gram) from Sigma-Aldrich, whereas the known $Re(bpy)(CO)_3Cl$ catalyst is $250 for 1 g at STREM Inc. In addition, benzil is a simple enough molecule that fine-tuning its electronics and sterics through functionalization does not provide a difficult challenge for synthetic chemists.

Ghobadi showed a reversible reduction of benzil at -1.56 V referenced to Ag/Ag^+ which becomes irreversible under carbon dioxide.[40] When pyridine was added, the size of the peak increases, although the extent to which peak height changed was not quantified. In this work, both benzil alone and benzil in conjunction with pyridine were explored as possible organic electrocatalysts in the reduction of carbon dioxide, and both options showed less overpotential required to reduce CO_2 compared to C_{60} which makes it an exciting potential candidate as a homogeneous organic electrocatalyst.

2.2. Buckminsterfullerene

2.2.1. Cyclic Voltammetry

The large conjugated π system present in buckminsterfullerene can be reversibly reduced multiple times and therefore lends itself to testing under CO_2 for electrocatalytic activity. However, it is relatively insoluble as a neutral species in common electrochemistry solvents such as acetonitrile. Rather, it is more soluble in nonpolar solvents, particularly arene solvents. Therefore, the less common electrochemical solvent 1,2-dichlorobenzene (ortho-dichlorobenzene, ODCB) was used. A plot comparing cyclic voltammograms of a solution of C_{60} under argon and carbon dioxide referenced to ferrocene is shown in Figure 2.3.

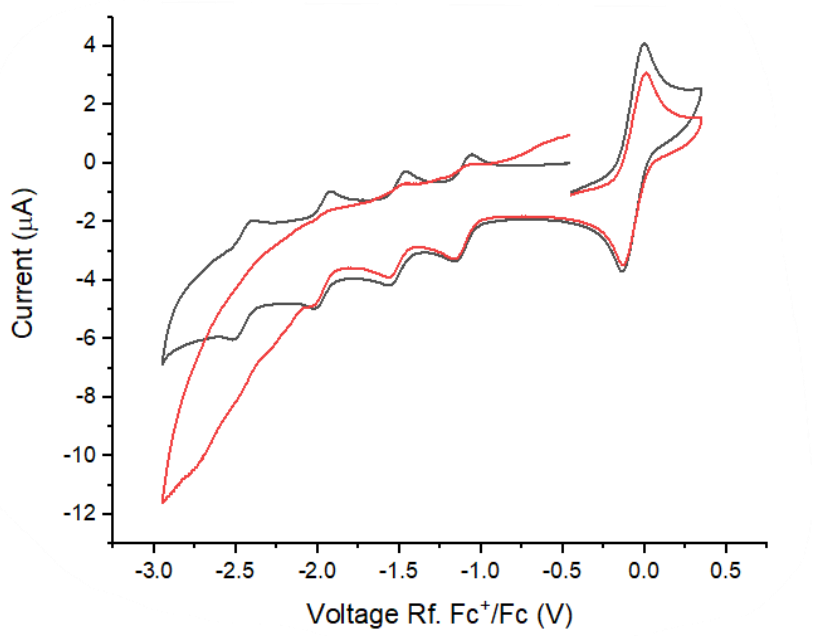

Figure 2.3. Representative cyclic voltammograms of C_{60} in ODCB with TBAH as a supporting electrolyte. Voltammograms were obtained for solutions under argon (black) and carbon dioxide (red) at 250 mV/s within the available solvent window.

When cyclic voltammograms were obtained under argon, four reversible reduction peaks were observed, each consistent with one electron being added to the C_{60}. Therefore, at room temperature in OCDB, we were able to observe the formation of C_{60}^{4-} from four reversible reductions of C_{60}. The spacing between each reduction is approximately 0.5 V. The replacement of the reversible peaks with irreversible behavior and a steady increase in irreversible reductive current when under carbon dioxide suggest a new chemical reaction with the trireduced species and therefore appreciable electrochemical activity. A steep increase in reductive current after the third reduction at -2 V suggests that if carbon dioxide reduction occurs, the species reducing CO_2 is $(C_{60})^{3-}$.

2.2.2. Infrared Spectroelectrochemistry

To further investigate the chemical changes taking place upon reduction of C_{60}, an IR-SEC of C_{60} under carbon dioxide was obtained (Figure 2.4).

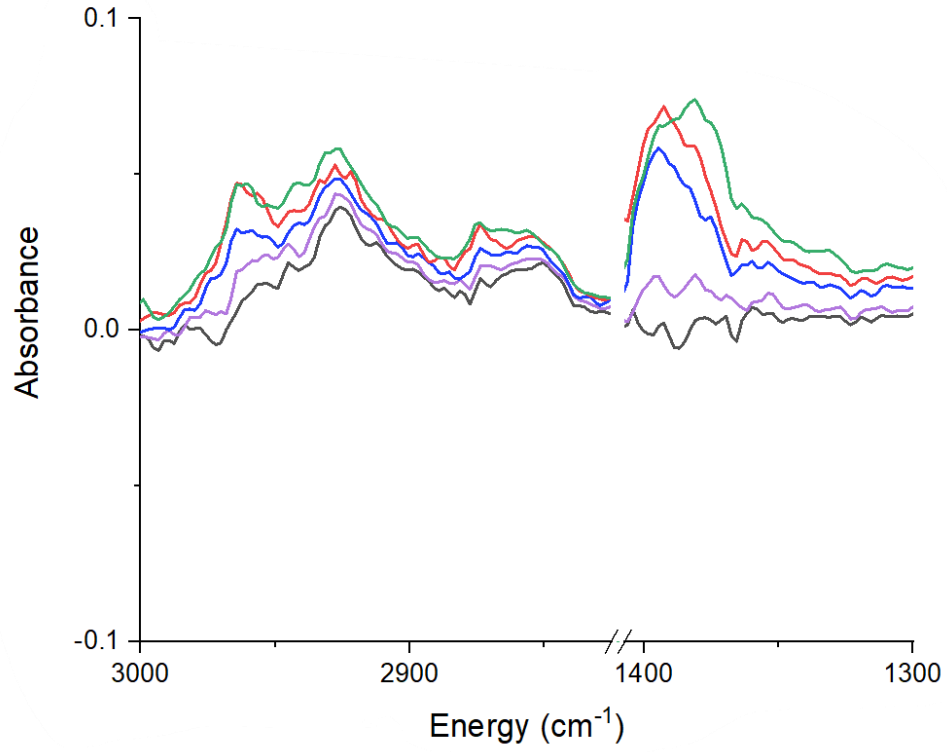

Figure 2.4. IR-SEC of C_{60} under carbon dioxide in ODCB. Spectra were obtained at 0 V (black), -1.8 V (purple), -1.9 V (blue), and -2.1 V taken twice (red and green in order).

Multiple peaks appear throughout the course of the IR-SEC experiment: without voltage applied, peaks are visible at 2926 cm^{-1} and 2873-2850 cm^{-1}. As voltage is applied, there is a slight but steady increase in the intensity of a peak at 2928 wavenumbers and in the range of 2873-2856 wavenumbers, as well as the rapid growth of a peak in the 1380-1400 wavenumber range. Although the growth of the peak at 1380-1400 may be carbon dioxide bound to C_{60}^{3-}, more experiments would be necessary to verify results. In addition, the catalysis was only observed after approximately -2 V versus ferrocene and did not show a large increase of catalytic current compared to the peak current under argon, and therefore C_{60} could not be considered a rapid catalyst. Therefore, we turned our attention towards benzil.

2.3. Benzil

2.3.1. Initial Cyclic Voltammograms

98% benzil was used for initial characterization experiments. Initial cyclic voltammograms in acetonitrile with TBAH as a supporting electrolyte under argon and carbon dioxide are shown in Figure 2.5.

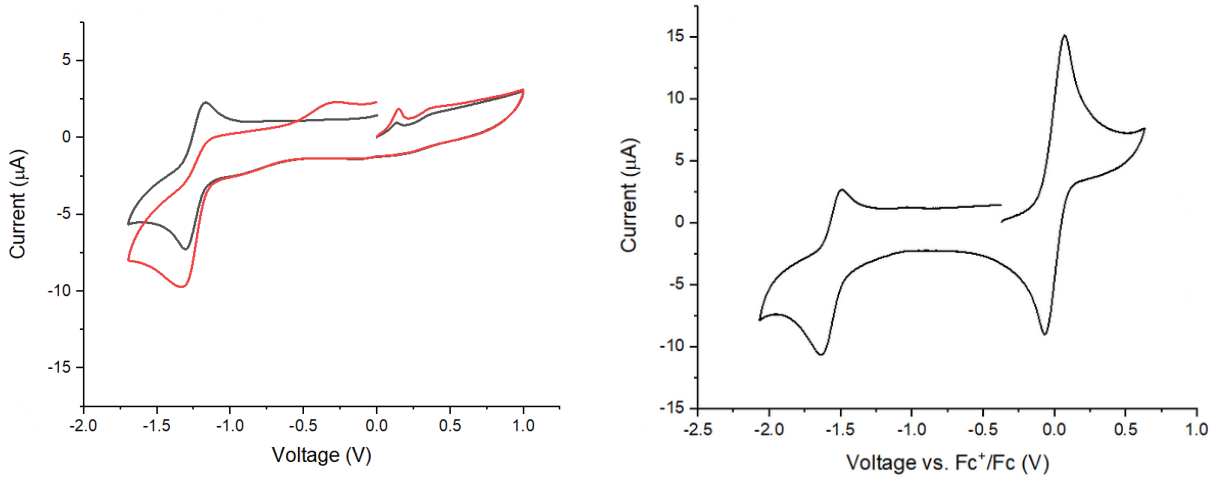

Figure 2.5. Representative CVs of benzil under argon and carbon dioxide. On the left, samples under argon (black) and carbon dioxide (red) are compared and show that a reversible redox process under argon becomes irreversible under carbon dioxide. On the right, 1.0 mM sublimed benzil was referenced to ferrocene under Ar to give a peak potential of the redox event versus ferrocene. Samples were dissolved in acetonitrile with TBAH as a supporting electrolyte.

A reversible reduction peak is seen at approximately -1.6 V versus Fc^{+}/Fc, which notably is a much smaller overpotential than seen with buckminsterfullerene if a reaction with carbon dioxide is occurring. Trials repeated under carbon dioxide showed the disappearance of the reverse oxidation peak. In the absence of any catalyst, carbon dioxide in acetonitrile shows no reduction in that range, suggesting at least qualitative catalysis of carbon dioxide reduction.

2.3.2. Purification of Stock Benzil

Stock benzil is available at 98% purity, containing benzoin as a possible impurity. Purified benzil was obtained through two different methods: recrystallization from ethanol or sublimation. Once purified, the benzil was characterized through cyclic voltammetry, infrared spectroscopy, and NMR spectroscopy. No major differences were observed between the two purified samples. The obtained NMR spectra of recrystallized and sublimed benzil is shown in Figure 2.6.

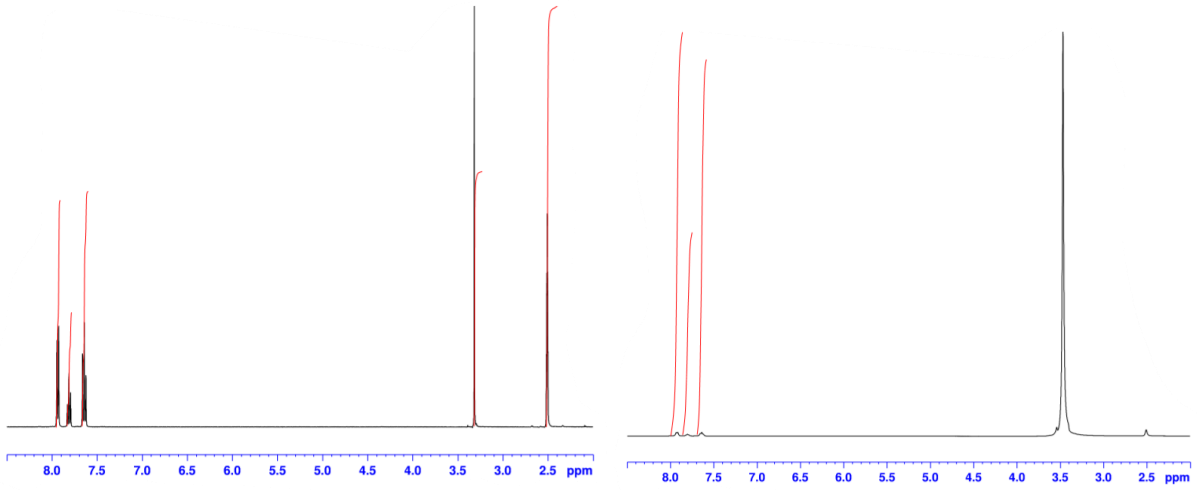

Figure 2.6. NMR of purified benzil. Recrystallized (left) and sublimed (right) benzil in DMSO-d^6. No major differences in species in solution were observed between the samples.

Because there are only hydrogens bound to the aromatic rings in benzil, the only protons show up are in a 1:2:2 ratio in the aromatic region; however, the sublimed sample is more dilute that the recrystallized sample which makes impurities less obvious The purification of benzil is an important step due to possible electrochemical activity of impurities like benzoin, which has a structure similar to benzil but has one ketone replaced with an alcohol.

The proposed electrochemical mechanism of benzil in argon includes two reversible reductions. A mechanism of forming oxalate via the reduction of benzil proposed by literature is shown below in Scheme 2.1.[39]

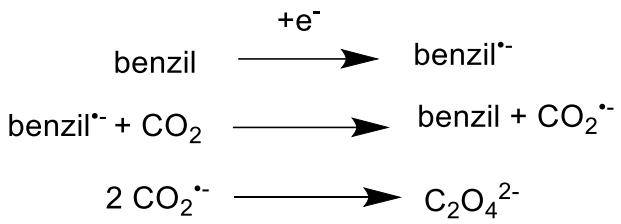

Scheme 2.1. Proposed mechanism for the electrocatalytic formation of oxalate via benzil.

Koshechko and Lopushanskaya also reference the disproportionation of the carbon dioxide radical anion into carbon monoxide and carbonate ion.[39] Currently, it is unclear why one path would be preferred over another, but further experimental and computational studies could elucidate the differences in transition state energies and overall thermodynamic favorability.

2.3.3. Infrared Spectroelectrochemistry

While cyclic voltammetry can yield myriad information about electrochemical activity, infrared spectroscopy can yield a much wider variety of structural information, allowing for the identification of both reactant species and following product species if a chemical reaction occurs, which is not as simple to accomplish with cyclic voltammetry. Infrared spectra were obtained for both recrystallized and sublimed benzil (Figure 2.7).

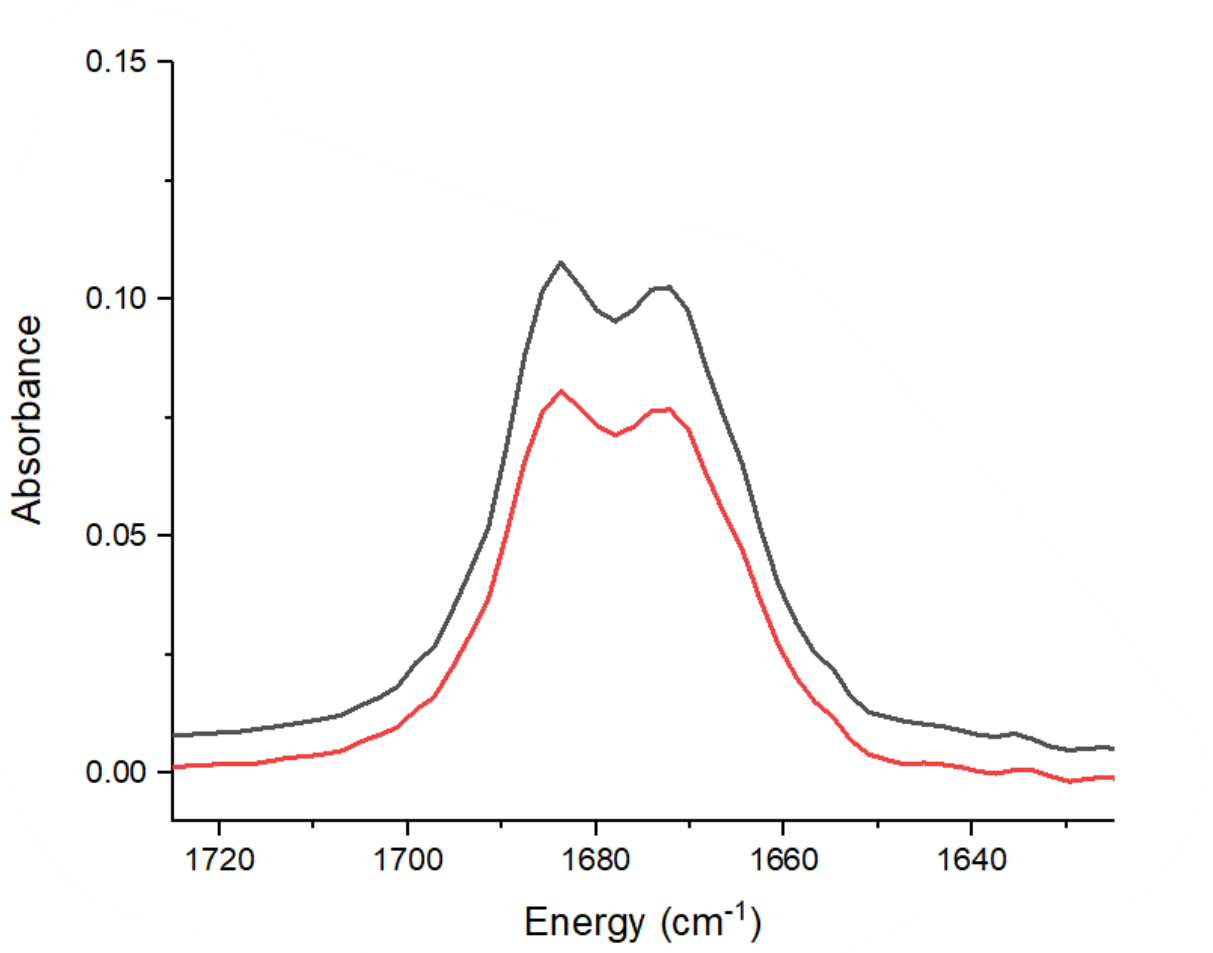

Figure 2.7. IR spectra of purified benzil samples. Samples of both recrystallized (black) and sublimed (red) were in acetonitrile and TBAH.

Both samples of purified benzil showed the same major peaks. From the spectra of purified benzil, peaks are observed at 1683-1670, 1596, 1213, and 1176 wavenumbers, which then were monitored over the course of tests for reactivity. Infrared spectroelectrochemistry was again used to observe changes in chemical structure and reactivity upon application of a voltage. Representative IR-SEC spectra of benzil under argon are shown in Figure 2.8.

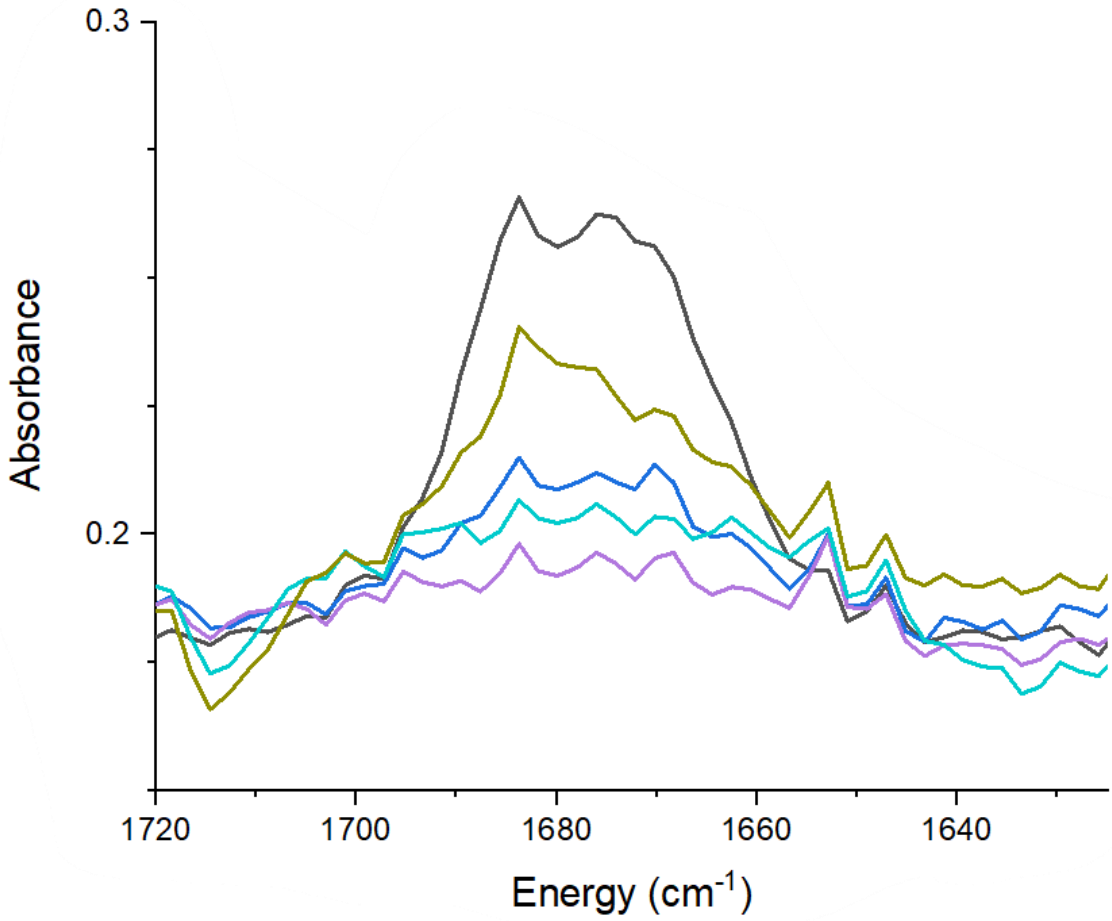

Figure 2.8. IR-SEC of benzil in acetonitrile with TBAH under argon. Voltammograms were obtained at 0 V (black), -1.2 V (blue), -1.5 V (purple), -2 V (cyan), and a return to 0 V afterwards (brown). Upon reoxidation, carbonyl peaks were observed to grow back in, indicating a reversible reduction/oxidation process.

The disappearance of the peak in the 1670-1683 cm^{-1} range gives a good reference for identifying the reduction of neutral benzil. We were not able to identify peaks corresponding to the reduced carbonyls of benzil anion in the IR-SEC spectra which may be because of interference in the 1350-1500 cm^{-1} region from the TBAH/acetonitrile solvent. Under carbon dioxide a second set of IR-SEC spectra were obtained (Figure 2.9).

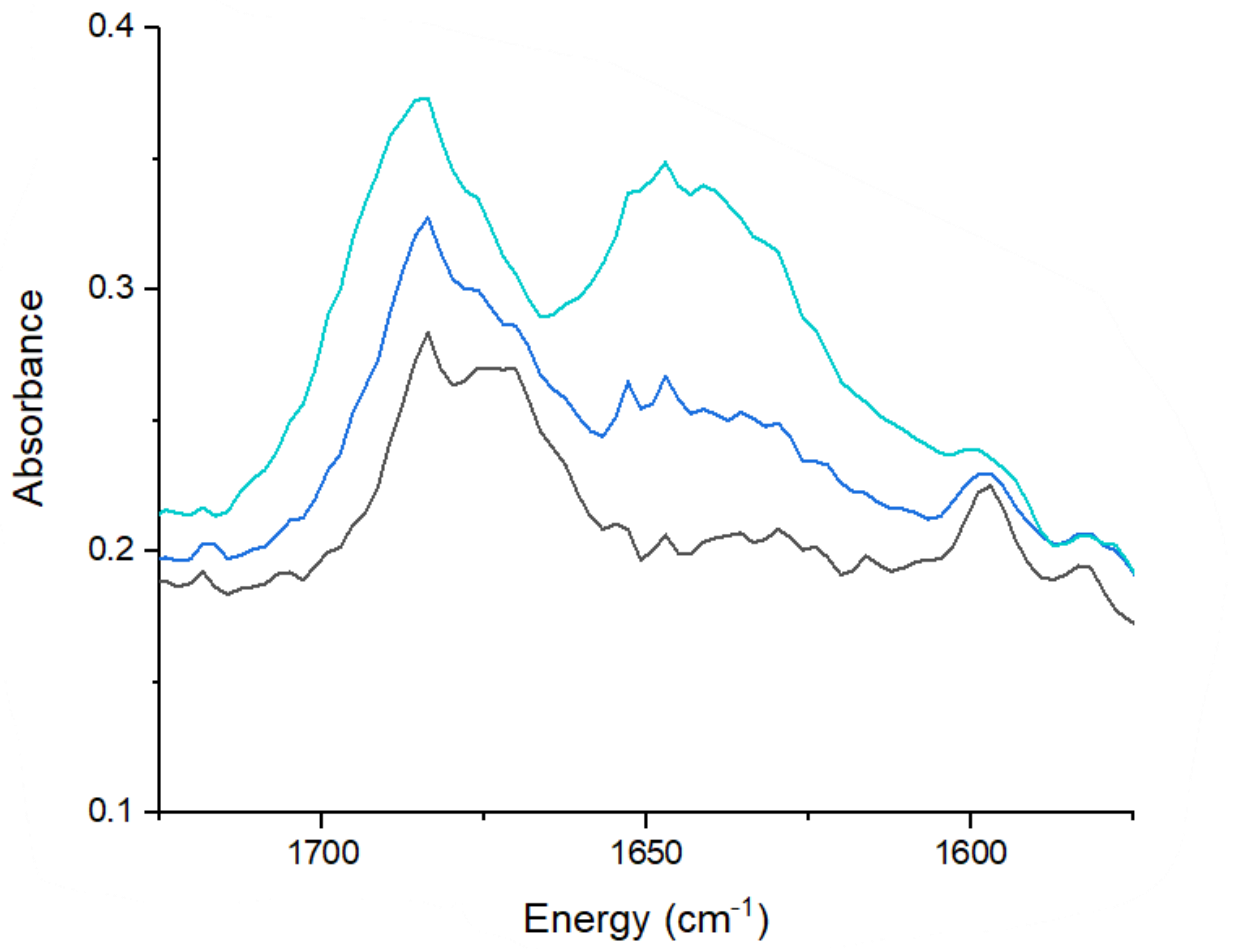

Figure 2.9. IR-SEC of benzil under CO_2 in acetonitrile and TBAH. Voltages of 0 V (black), -1 V (blue), and -1.2 V (cyan) were applied.

In contrast to the results of the IR-SEC under argon, when under carbon dioxide the peak at 1683 increases and changes shape as voltage becomes more negative, and an additional peak at 1647 cm^{-1} appears as well, likely the due to products of CO_2 reduction. That neutral benzil gradually disappears under a voltage and inert gas is not a difficult conclusion to reach, the observation of peak growth under carbon dioxide is an exciting discovery. Under carbon dioxide any reduced benzil may react with carbon dioxide to yield neutral benzil, as well as a product of

catalytic reduction marked by the appearance of a new peak at 1647 wavenumbers, potentially oxalate or oxalic acid if it became protonated.

2.2.4. Cyclic Voltammetry in the Presence of Pyridine

Ghobadi et al. combine benzil with pyridine in their work, giving evidence that catalytic activity and the production of isonicotinic acid is observed through addition of a carboxylate group to the *para* position of the pyridine ring, which was corroborated through NMR and FT-IR spcetroscopy.[40] The authors propose two cooperative catalytic cycles: the reduction of carbon dioxide by the monoreduced benzil radical anion to yield neutral benzil and monoreduced carbon dioxide; and the reduction of pyridine to an anion by the monoreduced carbon dioxide species to yield neutral carbon dioxide which can then participate in the first catalytic cycle again. A scheme of the proposed mechanism is shown in Scheme 2.2.

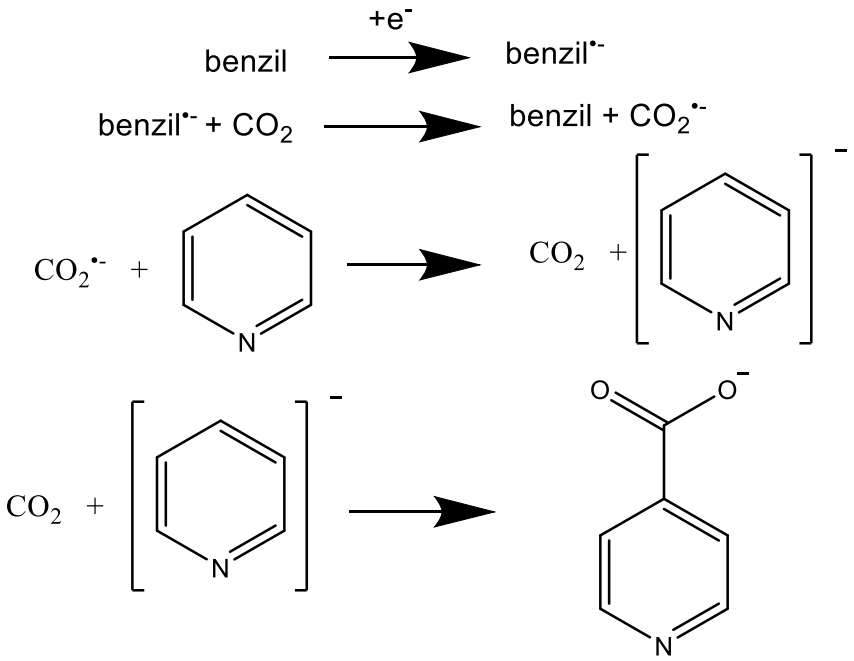

Scheme 2.2. Proposed mechanism for the production of isonicotinic acid.

To test those results, CVs were obtained for pyridine, benzil, and a qualitative mix of 1.0 mM benzil and added pyridine. Cyclic voltammograms of pyridine in ACN/TBAH showed no electrochemical activity under either argon or carbon dioxide, meaning that any catalytic activity from a combination of the two small molecules in solution would be due to either catalysis of only benzil or a multimolecular reaction involving both pyridine and benzil. Cyclic voltammograms of benzil compared to cyclic voltammograms of solutions containing both benzil and pyridine showed that peak height changed significantly, suggesting that pyridine plays a role in an electrochemical process that involves benzil and CO_2 as well (Figure 2.10).

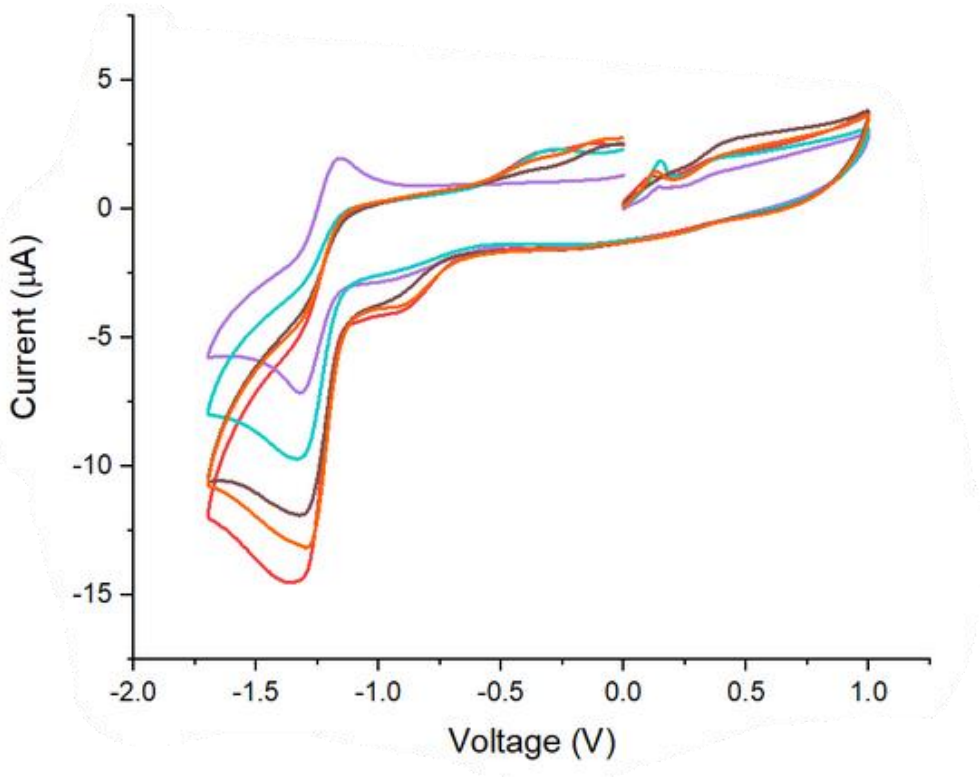

Figure 2.10. Cyclic voltammograms of benzil in different solution conditions. Here, cyclic voltammograms were obtained using a Pine Instruments WaveNow Potentiostat. All solutions use a dimethylformamide solvent and TBAH as a supporting electrolyte. Solutions used were benzil without pyridine under Ar (pink) or CO_2 (teal) or benzil with increasing amounts of pyridine under CO_2 (brown, orange, and red). As more pyridine is added, the magnitude of the peak reductive current at ~-1.3 V increases while the peak remains at the same approximate potential.

Having concluded that benzil reacts with carbon dioxide on its own, the increase in reductive current leads to the conclusion that pyridine acts as another catalytically active species within the same catalytic mechanism that includes benzil. To gain a better understanding of the reaction taking place, a more quantitative study on the effects of pyridine concentration was pursued. Representative cyclic voltammograms obtained from the study are shown in Figure 2.11.

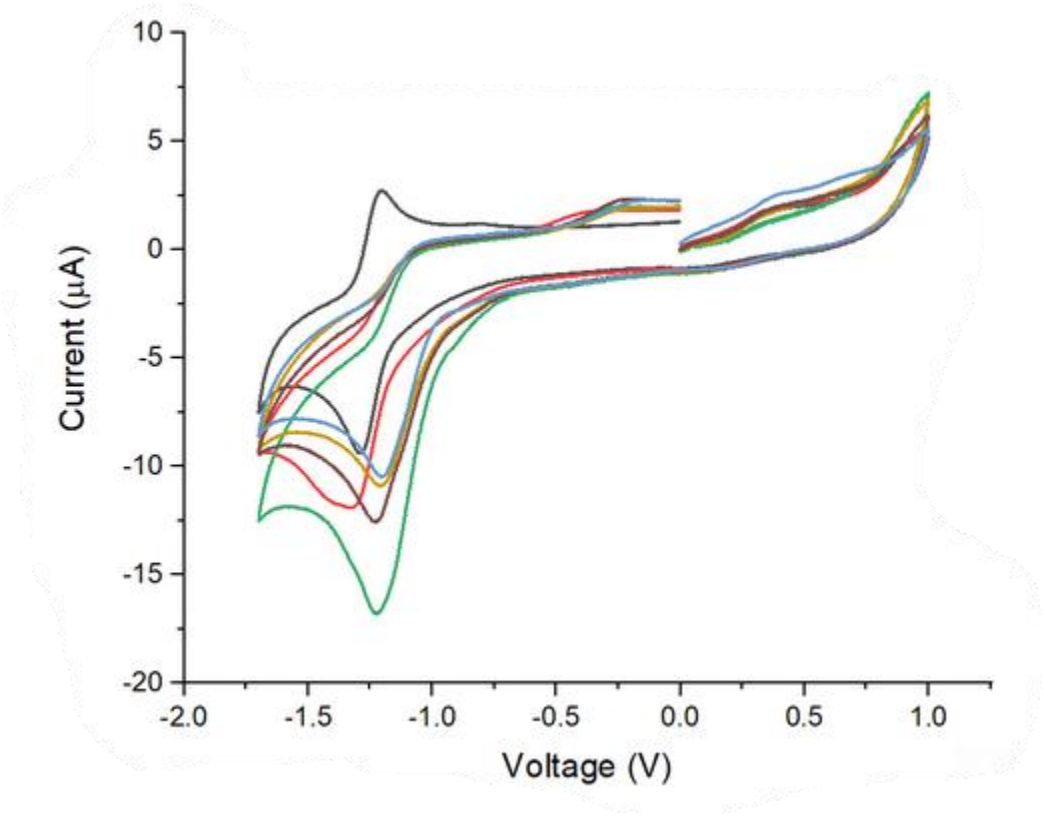

Figure 2.11. Cyclic voltammograms of benzil and pyridine in acetonitrile and TBAH. Solutions with a constant concentration of 1.0 mM benzil contained 0 mM (red), 1.0 mM (green), 1.99 mM (orange), 4.98 mM (brown), and 9.96 mM (blue) pyridine under carbon dioxide, compared to a solution of benzil in solvent alone under argon (black).

Surprisingly, there seemed to be no correlation between the height of the current peak and the concentration of pyridine in solution. There may be several explanations for the discrepancy between the studies: adventitious air or water may have caused the increase in current seen by

Ghobadi and our initial study; the concentration of benzil could have been a limiting factor in the study where pyridine was well-quantified; or the reaction taking place in solution may not follow the mechanism proposed by Ghobadi et al.

2.4. Conclusions and Future Directions

Initial investigations into benzil as an electrocatalyst showed significant promise for several reasons. Its bulk availability makes it an attractive target for both upscaling as well as the possibility of synthesizing benzil derivatives to optimize its catalytic activity. Derivatives of benzil are commercially available and attainable to synthesize; the possibility of tuning electronics or sterics of benzil—by adding electron donating or withdrawing groups for electronic changes or sterically bulky groups for steric changes—to reach more efficient catalysis is an attractive possibility which should be explored in the future.

An investigation into the electrocatalytic activity of C_{60} showed that although multiple reversible reductions are observed under argon which become irreversible under carbon dioxide, little catalytic activity seems to be observed other than a possible binding of CO_2 to the triply reduced fullerene. To fully understand the transformations that are taking place as well as the interactions of C_{60}—or lack thereof—with carbon dioxide, more data is needed. If the peak observed growing in the IR-SEC could be isolated or characterized, then a more informed conclusion could be drawn and further steps may be called for.

There are still many analytical tests possible to explore the catalytic activity of unmodified benzil. Voltage applied to a sample of benzil in deuterated solvent under carbon dioxide would allow for direct characterization of products formed through electrocatalysis. Finding the stability—or relatedly, the turnover number—of benzil as a catalyst is also an important factor to consider when determining its viability as an electrocatalyst, as even a catalyst that causes a

reaction to proceed thousands of times faster is not useful if it can only catalyze a few reactions before decomposing. Although the increase in current was observed upon addition of pyridine to a benzil solution showed an increase in reductive current, a quantitative study with the concentration of pyridine showed a lack of a trend between the concentration of pyridine present and the peak current. Further studies such as IR-SEC data would improve the quality of the conclusions that can be made from available results. In addition, the possibilities of using benzil as an electrocatalyst for carboxylating pyridines is attractive as an additional avenue for converting and incorporating carbon dioxide into more useful species.

Chapter 3. Experimental Methods

3.0.1. General Methods

Cyclic voltammograms were obtained from an eDAQ ER466 Integrated Potentiostat System unless otherwise specified. All NMR spectra were obtained on a Bruker Ascend 400 MHz NMR with an Avance Neo console and using Bruker TopSpin 4.0.7 software. Infrared and infrared spectroelectrochemistry spectra were obtained using an ABB FT-IR FTLA 2000 infrared spectrometer. For IR spectra, a demountable liquid cell with KBr windows was used. For IR-SEC, an optically transparent thin-layer electrochemical (OTTLE) cell with CaF_2 windows was used. The working electrode and counter electrodes were Pt mesh, and the pseudoreference electrode was a Ag wire. Analysis of voltammograms and spectral data was performed using Origin version 2018b (OriginLab, Northhampton, MA). Tetrabutylammonium hexafluorophosphate (TBAH) was recrystallized from HPLC-grade methanol and dried in a vacuum oven overnight prior to use.

3.1 Cyclic Voltammograms

A stock of tetrabutylammonium hexafluorophosphate (TBAH) in acetonitrile (ACN) (3.8744 g per 100 mL) was made to yield a 0.100 M stock. This solution was used for all cyclic voltammograms unless otherwise specified. Degassing was accomplished through sparging with the specified gas for 2-3 minutes between obtained cyclic voltammograms. For all trials, counter electrodes were platinum and all pseudoreference electrodes were silver wire. Acetonitrile, triethylamine, benzoic acid, acetic acid, trifluoroacetic acid, phenol, and pyridine were used as received from commercial suppliers.

3.1.1. Initial *fac*-Re(PyBimH)$(CO)_3$Cl Cyclic Voltammograms

fac-Re(PyBimH)$(CO)_3$Cl (**1**) (0.0129 g, 2.52 mM) was dissolved in 10.0 mL of ACN/TBAH stock solution. Cyclic voltammograms of the ACN/TBAH mixture in the absence of **1** were first obtained to find the appropriate solvent window. Samples transferred to the glass vial used for cyclic voltammetry were 1.5-2.0 mL aliquots. A glassy carbon working electrode, platinum counter electrode, and silver reference electrode were attached to the potentiostat and placed in solution. Samples were degassed with argon or carbon dioxide prior to each run. Cyclic voltammograms were obtained at a sweep rate of 250 mV/s with a voltage range of -2500 to +500 mV.

3.1.2 Scan Rate Study for *1*

1 (0.0125 g, 2.44 mM) was dissolved in 10.0 mL of ACN/TBAH. Samples placed into the cyclic voltammetry glass vial were 1.5-2.0 mL aliquots. The electrodes used were either platinum or glassy carbon for the working electrode. Samples were degassed with argon prior to each run. Cyclic voltammograms were obtained in the voltage range of -2500 to +500 mV, with scan rates

of either 250, 500, and 1000 mV/s with a platinum working electrode or 100, 250, 500, and 1000 mV/s with a glassy carbon electrode.

3.1.3. Cyclic Voltammograms of *1* in HAT Reaction Study

1 (16.3 mg) was dissolved in 10.0 mL of stock 0.1 M TBAH/ACN solution. The voltage range used was -1800 to +800 mV at a scan rate of 250 mV/s. Platinum was used as the working electrode.

3.1.4. Cyclic Voltammograms of Benchmark Acids

Benchmark acids were dissolved in stock 0.1 M TBAH/ACN solutions with a qualitative amount of ferrocene as an external reference. Platinum was used for all samples as the working electrode. All scan rates were 250 mV/s. To protonate piperidine, 2.05 μL of concentrated hydrochloric acid were added to the sample solution before cyclic voltammograms were obtained. A list of the voltage ranges and concentrations of solute used is given in Table 3.1.

Table 3.1. Concentration, Voltage Range, and Notes for Benchmark Acid Samples

Species Tested	Concentration (mM)	Voltage Range (mV)
Acetic acid	2.50	-1600 to +800
Anilinium hydrochloride	2.60	-1800 to +800
Benzoic acid	2.21	-1800 to +500
Morpholinium hydrochloride	2.50	-1800 to +800
Piperidinium hydrochloride	2.50	-1800 to +800
Pyridinium hydrochloride	2.49	-1800 to +800
Trifluoroacetic acid	2.50	-1600 to +800

3.1.5. Buckminsterfullerene Cyclic Voltammograms

TBAH (0.3885 g, 0.100 M) was dissolved in 10.0 mL of ODCB and cyclic voltammograms were obtained to observe the solvent window. A qualitative amount of C_{60} was then added and the solution was degassed with argon or carbon dioxide before obtaining cyclic voltammograms.

Glassy carbon was used as the working electrode. A qualitative amount of ferrocene was added to the solution as an external reference. Scans were obtained in the range of -3000 to +500 mV at a sweep rate of 250 mV/s.

3.1.6. Initial Cyclic Voltammograms of Benzil

Stock 0.1 M TBAH in ACN was used as a solvent and supporting electrolyte. Benzil (3.0 mg, 1.4 mM) was added to 10.0 mL of the solution mixture, and samples were degassed with either argon or carbon dioxide prior to each run. Scans were obtained in the range of -1600 to +1400 mV at a sweep rate of 250 mV/s. Glassy carbon was used as the working electrode.

3.1.7. Cyclic Voltammograms of Recrystallized Benzil

A qualitative amount of recrystallized benzil was dissolved in stock 0.1 M TBAH/ACN solution, with a qualitative amount of ferrocene as an external reference. Samples were degassed with argon or carbon dioxide prior to running trials. Scans were obtained in the range of -1700 to +1000 mV, with scan rates of 100, 250, 500, and 1000 mV/s.

3.1.8. Cyclic Voltammograms of Sublimed Benzil

Benzil (2.1 mg, 1.0 mM) was dissolved in 10.0 mL of stock 0.1 M TBAH/ACN solution. Glassy carbon was used as the working electrode. A qualitative amount of ferrocene was added to sample solutions as an external reference. Samples were degassed with argon prior to running trials. Scans were obtained in the range -1700 to +1000 mV at a scan rate of 250 mV/s.

3.1.9. Cyclic Voltammograms of Benzil in the Presence of Pyridine

Benzil (2.2 mg, 1.0 mM) was added to 10.0 mL of stock 0.1 M TBAH/ACN solution. Glassy carbon was used as the working electrode. Scans were obtained in the range of -1700 to

+1000 mV with a scan rate of 250 mV/s. Samples were degassed with either argon or carbon dioxide prior to each run. After obtaining three consistent cyclic voltammograms under argon and three consistent cyclic voltammograms under carbon dioxide, qualitative amounts of pyridine were added between sets of trials. Due to the number of times the solution was degassed, evaporation resulted in loss of solution volume and more sample solution had to be added.

Another set of cyclic voltammograms were obtained using quantitative amounts of pyridine added to solutions of ACN, TBAH, and benzil. Benzil (8.6 mg, 1.0 mM) was dissolved in 40.0 mL of stock ACN/TBAH, which was split into four 10.0 mL aliquots. Pyridine (0.81 μL, 1.0 mM; 1.61 μL, 1.99 mM; 4.03 μL, 4.98 mM; 8.06 μL, 9.96 mM) was added to the aliquots to make solutions of differing pyridine concentration. Glassy carbon was used as the working electrode. The voltage range used was -1700 mV to +1000 V at a sweep rate of 250 mV/s.

3.2. Syntheses and Purifications

3.2.1. Synthesis of *fac*-Re(PyBimH)(CO)$_3$Cl

Complex **1**, *fac*-Re(PyBimH)(CO)$_3$Cl, was synthesized in one step based on the synthesis of Warren et al[22]. Re(CO)$_5$Cl (160.1 mg, 0.4426 mmol) and PyBimH (137.4 mg, 0.663 mmol) were dissolved in 20 mL of toluene, then the mixture was refluxed for 50 minutes. The product was precipitated in hexanes and further precipitated in a freezer for 72 hours. The resultant precipitate and mother liquor were washed through a glass frit with ice-cooled hexanes and vacuum-dried to yield the yellow powder *fac*-Re(PyBimH)(CO)$_3$Cl product (0.2469 g, 90.54% yield).

3.2.2. Synthesis of Amine Hydrochloride Salts

Anilinium Hydrochloride

Aniline (4.00 mL, 43.7 mmol) was placed in an evaporating dish and mixed with concentrated hydrochloric acid (4.361 mL, 52.33 mmol). The reaction mixture was left overnight and washed with diethyl ether to yield the light purple solid product.

Imidazolium Hydrochloride

Imidazole (0.1666 g, 2.447 mmol) was combined with concentrated hydrochloric acid (196.3 μL, 2.356 mmol) and left to evaporate.

3.2.3. Purification of Benzil by Recrystallization

Boiling ethanol was added to stock benzil (3.9 g) until the benzil was completely dissolved, then the solution was allowed to cool to room temperature, yielding a precipitate of yellow spear-shaped crystals. The mixture was washed through a glass frit through vacuum filtration using cold ethanol. Crystals were left overnight in the glass frit to dry over time while covered with Parafilm, also leaving the mother liquor in the sidearm flask. The resulting dried crystal product were transferred to a glass vial (3.3154 g, 85% yield).

3.2.4. Purification of Benzil by Sublimation

Unpurified benzil (2 g) was placed in a sublimator equipped with ice in the cold finger and heated to approximately 95°C under static vacuum for one week. Vacuum was created using the house vacuum line on the fume hood. A fine, crystalline, yellow powder was scraped from the cold finger and surrounding area of the sublimating apparatus.

3.3. Infrared Spectra

3.3.1. *fac*-Re(PyBimH)(CO)$_3$Cl

fac-Re(PyBimH)(CO)$_3$Cl (14.5 mg, 2.83 mM) was dissolved in 10.0 mL ACN and split into two 5.0-mL aliquots. Triethylamine (7.9 μL, 5.6 mM) was added to one aliquot. Neither sample was degassed. Stock acetonitrile was used to obtain a baseline.

3.3.2. Recrystallized and Sublimed Benzil

A stock solution of 0.1 M TBAH/ACN degassed with argon was used to obtain a baseline. Solutions of recrystallized (2.1 mg, 2.0 mM) and sublimed (2.3 mg, 2.0 mM) were dissolved in 5.0 mL aliquots of stock TBAH/ACN solutions.

3.4. Infrared Spectroelectrochemistry Spectra

3.4.1. *fac*-Re(PyBimH)(CO)$_3$Cl

Stock 0.1 M TBAH in ACN was used to obtain a baseline. A solution was made from **1** (0.0159 g, 3.10 mM) in 10.0 mL of stock TBAH/ACN and split into two 5.0 mL aliquots, which were degassed with either argon or carbon dioxide prior to obtaining spectra.

3.4.2. Buckminsterfullerene

A quantitative amount of buckminsterfullerene was dissolved in 10.0 mL of *o*-dichlorobenzene and the sample was degassed with carbon dioxide prior to obtaining a spectrum. Stock *o*-dichlorobenzene was used to obtain a baseline.

3.4.3. Sublimed Benzil

A stock solution of 0.1 M TBAH/ACN degassed with argon was used to obtain a baseline. Sublimed benzil (20.9 mg, 9.94 mM) was dissolved in 10.0 mL of stock TBAH/ACN solution. Two aliquots were degassed with either argon or carbon dioxide.

3.5. Nuclear Magnetic Resonance (NMR) Spectra of Recyrstallized and Sublimed Benzil

Samples of recrystallized and sublimed benzil were dissolved in dimethylsulfoxide-d^6. Spectra were compiled from 16 scans.

References

1. Dempsey, J. L.; Esswein, A. J.; Manke, D. R.; Rosenthal, J.; Soper, J. D.; Nocera, D. G., Molecular Chemistry of Consequence to Renewable Energy. *Inorg. Chem.* **2005,** *44* (20), 6879-6892.
2. Hammes-Schiffer, S., When electrons and protons get excited. *Proc. Natl. Acad. Sci.* **2011,** *108* (21), 8531-8532.
3. Grice, K. A.; Kubiak, C. P., Recent Studies of Rhenium and Manganese Bipyridine Carbonyl Catalysts for the Electrochemical Reduction of CO_2. In *CO_2 Chem.*, 2014; pp 163-188.
4. Grice, K. A.; Gu, N. X.; Sampson, M. D.; Kubiak, C. P., Carbon monoxide release catalysed by electron transfer: electrochemical and spectroscopic investigations of [Re(bpy-R)$(CO)_4$](OTf) complexes relevant to CO_2 reduction. *Dalton Trans.* **2013,** *42* (23).
5. Grice, K. A.; Saucedo, C.; Sovereign, M. A.; Cho, A. P., The Electrochemical Behavior of Early Metal Metallocene Cp_2MCl_2 Complexes under CO_2. *Electrochim. Acta* **2016,** *218*, 110-118.
6. Sampson, M. D.; Nguyen, A. D.; Grice, K. A.; Moore, C. E.; Rheingold, A. L.; Kubiak, C. P., Manganese Catalysts with Bulky Bipyridine Ligands for the Electrocatalytic Reduction of Carbon Dioxide: Eliminating Dimerization and Altering Catalysis. *J. Am. Chem. Soc.* **2014,** *136* (14), 5460-5471.
7. Grice, K. A., Carbon dioxide reduction with homogenous early transition metal complexes: Opportunities and challenges for developing CO_2 catalysis. *Coord. Chem. Rev.* **2017,** *336*, 78-95.
8. Sung, S.; Li, X.; Wolf, L. M.; Meeder, J. R.; Bhuvanesh, N. S.; Grice, K. A.; Panetier, J. A.; Nippe, M., Synergistic Effects of Imidazolium-Functionalization on fac-Mn$(CO)_3$ Bipyridine Catalyst Platforms for Electrocatalytic Carbon Dioxide Reduction. *J. Am. Chem. Soc.* **2019,** *141* (16), 6569-6582.

9. Mayer, J. M., Understanding Hydrogen Atom Transfer: From Bond Strengths to Marcus Theory. *Acc. Chem. Res.* **2011,** *44* (1), 36-46.
10. Warren, J. J.; Tronic, T. A.; Mayer, J. M., Thermochemistry of Proton-Coupled Electron Transfer Reagents and its Implications. *Chem. Rev.* **2010,** *110* (12), 6961-7001.
11. Kissinger, P. T.; Heineman, W. R., Cyclic voltammetry. *J. Chem. Ed.* **1983,** *60* (9).
12. Pavlishchuk, V. V.; Addison, A. W., Conversion constants for redox potentials measured versus different reference electrodes in acetonitrile solutions at 25°C. *Inorg. Chim. Acta* **2000,** *298* (1), 97-102.
13. Noviandri, I.; Brown, K. N.; Fleming, D. S.; Gulyas, P. T.; Lay, P. A.; Masters, A. F.; Phillips, L., The Decamethylferrocenium/Decamethylferrocene Redox Couple: A Superior Redox Standard to the Ferrocenium/Ferrocene Redox Couple for Studying Solvent Effects on the Thermodynamics of Electron Transfer. *J. Phys. Chem. B* **1999,** *103* (32), 6713-6722.
14. Raamat, E.; Kaupmees, K.; Ovsjannikov, G.; Trummal, A.; Kütt, A.; Saame, J.; Koppel, I.; Kaljurand, I.; Lipping, L.; Rodima, T.; Pihl, V.; Koppel, I. A.; Leito, I., Acidities of strong neutral Brønsted acids in different media. *J. Phys. Org. Chem.* **2013,** *26* (2), 162-170.
15. Tshepelevitsh, S.; Kütt, A.; Lõkov, M.; Kaljurand, I.; Saame, J.; Heering, A.; Plieger, P. G.; Vianello, R.; Leito, I., On the Basicity of Organic Bases in Different Media. *Eur. J. Org. Chem.* **2019,** *2019* (40), 6735-6748.
16. Kütt, A.; Leito, I.; Kaljurand, I.; Sooväli, L.; Vlasov, V. M.; Yagupolskii, L. M.; Koppel, I. A., A Comprehensive Self-Consistent Spectrophotometric Acidity Scale of Neutral Brønsted Acids in Acetonitrile. *J. Org. Chem.* **2006,** *71* (7), 2829-2838.
17. Kaljurand, I.; Kütt, A.; Sooväli, L.; Rodima, T.; Mäemets, V.; Leito, I.; Koppel, I. A., Extension of the Self-Consistent Spectrophotometric Basicity Scale in Acetonitrile to a Full Span of 28 pK_a Units: Unification of Different Basicity Scales. *J. Org. Chem.* **2005,** *70* (3), 1019-1028.
18. Ding, F.; Smith, J. M.; Wang, H., First-Principles Calculation of pK_a Values for Organic Acids in Nonaqueous Solution. *J. Org. Chem.* **2009,** *74* (7), 2679-2691.
19. Hawecker, J.; Lehn, J.-M.; Ziessel, R., Photochemical and Electrochemical Reduction of Carbon Dioxide to Carbon Monoxide Mediated by (2,2'-Bipyridine)tricarbonylchlororhenium(I) and Related Complexes as Homogeneous Catalysts. *Helv. Chim. Acta* **1986,** *69* (8), 1990-2012.
20. Johnson, E. M.; Haiges, R.; Marinescu, S. C., Covalent-Organic Frameworks Composed of Rhenium Bipyridine and Metal Porphyrins: Designing Heterobimetallic Frameworks with Two Distinct Metal Sites. *ACS Appl. Mater. Interfaces* **2018,** *10* (44), 37919-37927.
21. Talukdar, K.; Sinha Roy, S.; Amatya, E.; Sleeper, E. A.; Le Magueres, P.; Jurss, J. W., Enhanced Electrochemical CO_2 Reduction by a Series of Molecular Rhenium Catalysts Decorated with Second-Sphere Hydrogen-Bond Donors. *Inorg. Chem.* **2020,** *59* (9), 6087-6099.
22. Sinha, S.; Berdichevsky, E. K.; Warren, J. J., Electrocatalytic CO_2 reduction using rhenium(I) complexes with modified 2-(2′-pyridyl)imidazole ligands. *Inorg. Chim. Acta* **2017,** *460*, 63-68.
23. Mabbott, G. A., An introduction to cyclic voltammetry. *J. Chem. Ed.* **1983,** *60* (9).
24. McCarthy, B. D.; Martin, D. J.; Rountree, E. S.; Ullman, A. C.; Dempsey, J. L., Electrochemical Reduction of Brønsted Acids by Glassy Carbon in Acetonitrile—Implications for Electrocatalytic Hydrogen Evolution. *Inorg. Chem.* **2014,** *53* (16), 8350-8361.
25. Costentin, C.; Savéant, J.-M.; Tard, C., Catalysis of CO_2 Electrochemical Reduction by Protonated Pyridine and Similar Molecules. Useful Lessons from a Methodological Misadventure. *ACS Energy Lett.* **2018,** *3* (3), 695-703.

26. Eckert, F.; Leito, I.; Kaljurand, I.; Kütt, A.; Klamt, A.; Diedenhofen, M., Prediction of acidity in acetonitrile solution with COSMO-RS. *J. Comput. Chem.* **2009,** *30* (5), 799-810.
27. Espinoza, E. M.; Clark, J. A.; Soliman, J.; Derr, J. B.; Morales, M.; Vullev, V. I., Practical Aspects of Cyclic Voltammetry: How to Estimate Reduction Potentials When Irreversibility Prevails. *J. Electrochem. Soc.* **2019,** *166* (5), H3175-H3187.
28. Machan, C. W.; Sampson, M. D.; Chabolla, S. A.; Dang, T.; Kubiak, C. P., Developing a Mechanistic Understanding of Molecular Electrocatalysts for CO_2 Reduction using Infrared Spectroelectrochemistry. *Organometallics* **2014,** *33* (18), 4550-4559.
29. Lense, S.; Grice, K. A.; Gillette, K.; Wolf, L. M.; Robertson, G.; McKeon, D.; Saucedo, C.; Carroll, P. J.; Gau, M., Effects of Tuning Intramolecular Proton Acidity on CO_2 Reduction by Mn Bipyridyl Species. *Organometallics* **2020,** *39* (13), 2425-2437.
30. Friedlingstein, P.; Solomon, S., Contributions of past and present human generations to committed warming caused by carbon dioxide. *Proc. Natl. Acad. Sci.* **2005,** *102* (31), 10832-10836.
31. Finn, C.; Schnittger, S.; Yellowlees, L. J.; Love, J. B., Molecular approaches to the electrochemical reduction of carbon dioxide. *Chem. Commun.* **2012,** *48* (10), 1392-1399.
32. Gennaro, A.; Isse, A. A.; Savéant, J.-M.; Severin, M.-G.; Vianello, E., Homogeneous Electron Transfer Catalysis of the Electrochemical Reduction of Carbon Dioxide. Do Aromatic Anion Radicals React in an Outer-Sphere Manner? *J. Am. Chem. Soc.* **1996,** *118* (30), 7190-7196.
33. Pospíšil, L.; Bulíčková, J.; Hromadová, M.; Gál, M.; Civiš, S.; Cihelka, J.; Tarábek, J., Electrochemical conversion of dinitrogen to ammonia mediated by a complex of fullerene C_{60} and γ-cyclodextrin. *Chem. Commun.* **2007,** (22), 2270-2272.
34. Kalsbeck, W. A.; Thorp, H. H., Electrochemical reduction of fullerenes in the presence of O_2 and H_2O: Polyoxygen adducts and fragmentation of the C_{60} framework. *J. Electroanal.* **1991,** *314* (1-2), 363-370.
35. Kroto, H. W.; Allaf, A. W.; Balm, S. P., C_{60}: Buckminsterfullerene. *Chem. Rev.* **2002,** *91* (6), 1213-1235.
36. Ryan, M. D.; Evans, D. H., Effect of metal ions on the electrochemical reduction of benzil in non-aqueous solvents. *J. Electroanal. Chem.* **1976,** *67* (3), 333-357.
37. Cheek, G. T., Electrochemical Investigations of Benzil in Nonaqueous Media. *ECS Trans.* **2014,** *64* (4), 145-149.
38. Stapelfeldt, H. E.; Perone, S. P., Electrochemical reduction of benzil in alkaline methanol-water solution. *Anal. Chem.* **2002,** *41* (4), 623-627.
39. Koshechko, V. G.; Lopushanskaya, V. A., Electrochemical conversion of carbon dioxide catalysed by benzil. *Theor. Exp. Chem.* **2006,** *42* (1), 33-36.
40. Ghobadi, K.; Zare, H. R.; Khoshro, H.; Jafari, A. A., Excellent electrocatalytic activity of benzil for direct reduction of CO_2 as well as indirect reduction of pyridine: A kinetic view of the electrocarboxylation process. *J. Energy Chem.* **2017,** *26* (3), 569-573.